Thermal effects of a novel picosecond infrared laser during ablation of *ex vivo* soft tissue and bone

Nathan Jowett, BSc (Physics), MD, FRCSC

Department of Otolaryngology – Head and Neck Surgery, McGill University, Montreal

April 2013

A thesis submitted to McGill University in partial fulfillment of the requirements of the degree of Master of Science in Otolaryngology – Head and Neck Surgery

For my mother, late father, and Professor Emeritus Werden J. Keeler

Abstract

Background: Despite significant advances in surgery over the last century, most surgical approaches necessitate cold steel instruments under the control of the surgeon's hand. Lasers provide a means of precise surgical ablation, but their clinical use has remained limited due to undesired thermal, free-radical producing, or mechanical effects causing significant cellular insult. A novel ultrafast, non-ionizing, picosecond infrared laser (PIRL) system has recently been developed, capable in theory of ablation with negligible thermal or mechanical collateral damage.

Objective: The purpose of this work is to provide the reader with an overview of laser-tissue interactions and laser ablation mechanisms in addition to presenting novel experimental data comparing heat generation during ablation of *ex vivo* porcine skin and chicken bone by conventional microsecond pulsed erbium doped yttrium aluminum garnet (Er:YAG) laser versus PIRL.

Methods: *Ex vivo* porcine skin and chicken bone was ablated with both Er:YAG laser and PIRL at fluence levels above ablation threshold. Temperature rises were determined using infrared thermography and compared using appropriate statistical methods. Ablation craters were assessed by means of digital microscopy.

Results: Mean peak rise in skin surface temperature for the Er:YAG laser and PIRL was 15.0°C and 1.68°C, respectively ($p < 0.001$). Mean peak rise in bone temperature for the Er:YAG laser and PIRL was 12.99°C and 1.56°C, respectively ($p < 0.008$). Ablation craters appeared similar on digital microscopy.

Conclusions: Types of laser ablation include photothermal, photochemical, plasma-mediated, and photomechanical. Material removal resulting from microsecond pulsed

Er:YAG laser and PIRL ablation occurs via photothermal vaporization, enhanced by photomechanical effects. The PIRL produces efficient tissue ablation with negligible heat generation due to thermal and acoustic confinement conditions that enhance secondary photomechanical material removal.

Résumé

Introduction: Malgré les avancées significatives dans la chirurgie, les approches chirurgicales nécessitent souvent des instruments en acier froid sous le contrôle de la main du chirurgien. Les lasers offrent un moyen de l'ablation chirurgicale précise, mais leur utilisation en chirurgie reste limitée en raison des effets indésirables thermiques, ionisants, ou mécaniques causant d'insultes cellulaires. Un système laser pulsé ultra-rapide, non-ionisant, infrarouge picoseconde (PIRL) a récemment été développé qui est capable, en théorie, de l'ablation avec les effets négligeables thermiques et acoustiques.

Objectif: Le but de ce travail est de fournir au lecteur une vue d'ensemble interactions laser-tissus et des mécanismes d'ablation par laser, en plus de présenter de nouvelles données expérimentales comparant la production de chaleur lors de l'ablation de la peau de porc et l'os de poulet *ex vivo* par laser pulsé microseconde à l'erbium dopé d'yttrium aluminium garnet (Er: YAG) par rapport au PIRL.

Méthodes: La peau de porc et l'os de poulet *ex vivo* a été ablatée par laser Er :YAG et par PIRL aux niveaux de fluence dessus du seuil d'ablation. Les hausses de température ont été mesurées et comparées à l'aide de méthodes statistiques appropriées. Cratères d'ablation ont été évalués à l'aide de la microscopie numérique.

Résultats : Les hausses moyennes des pics de température sur la surface de la peau de cochon pendant l'ablation de laser Er:YAG et PIRL étaient de 15,0°C et de 1,68°C, respectivement ($p < 0,001$). Les hausses moyennes des pics de température osseuse pour l'ablation avec le laser Er: YAG et PIRL était 12,99°C et 1,56°C, respectivement ($p < 0,008$). Cratères d'ablation semblaient similaires à l'aide de la microscopie numérique.

Conclusions : Les types d'ablation par laser comprennent photochimique, photomécanique, plasma-médiée, et photomécaniques. L’enlèvement de matière résultant de l’ablation par laser pulsé microseconde Er: YAG et par PIRL se produit par voie photothermique, renforcée par des effets secondaire photomécaniques. Le PIRL produit l’ablation du tissu efficace en raison des conditions de confinement thermique et acoustique qui augmentent l'enlèvement de matière par mécanisme secondaire photomécanique.

Table of Contents

Preface

Contributions of authors

Dr. Nathan Jowett was responsible for the literature review in its entirety, the concept, design, data collection, and analysis of results of both manuscripts, and the drafting of both manuscripts. Dr. Wolfgang Wöllmer assisted in the conception and data collection for the first manuscript. Data collection was conducted at the University Medical Centre Hamburg – Eppendorf. The literature review, results interpretation, statistical analysis, discussion and conclusion were the work of Dr. Jowett. Dr. Alex Mlynarek provided supervision, guidance, clinical relevance expertise, and review of this thesis. Dr. Paul Wiseman provided supervision, guidance, basic ultrafast laser expertise, and review of this thesis.

The design and conception of the original scope of this Master's thesis, which involved longitudinal live animal experiments, was the work of Dr. Jowett. Research protocols, grants, and live animal use protocols for the originally planned work were written by Dr. Jowett, and will now form the basis of a PhD thesis.

Claim of originality

The original idea for the need to measure heat generation during PIRL ablation was the work Dr. Nathan Jowett and Dr. Wolfgang Wöllmer. The design of the experiments presented in this thesis, with direct comparison to erbium doped yttrium aluminum garnet (Er:YAG) laser ablation, was conceived by Dr. Nathan Jowett. No prior study has examined real-time heat generation during PIRL ablation.

Acknowledgements

Research, travel, and salary funding was provided by the Canadian Institutes of Health Research (CIHR) via a Frederick Banting and Charles Best Master's Award, the McGill Department of Otolaryngology – Head and Neck Surgery via the Head and Neck Surgery Fund, the Canadian Institute of Photonic Innovations (CIPI) via a Technology Exploitation and Networking (TEN) Collaboration Grant, the American Academy of Otolaryngology (AAO) via a Centralized Otolaryngology Research Efforts (CORE) Resident Research Grant, the European Research Council (ERC) via an Advanced Investigator Grant, and the McGill Faculty of Medicine via the Graduate Program for International Travel and the Frank Litvack Fellowship for Clinician Scientists. I am deeply indebted to Prof. Saul Frenkiel, Ms. Joanna Aroutian and Ms. Ilhem Douagui for their immense support and help with securing funding for this project. I thank Dr. Bernard Segal for his support, advice, and excellent critical review of this work. I thank Dr. Alex Mlynarek for his guidance, teaching, and for his help with seeing this project through to its completion. I thank Dr. Paul Wiseman for his time and help with securing grant funding and collaborations, in addition to his guidance and support. I thank Dr. Wolfgang Wöllmer for his input into the design of this study and his invaluable help in securing use of the equipment necessary to complete it. I thank Prof. RJD Miller for welcoming me to collaborate with his Max Planck Research team in Hamburg, Germany. I thank Dr. Kresimir Franjic for his expertise with the beam profile of the PIRL. I acknowledge and thank Dr. Matthias Kraub of InfraTec GmBH for his help with generating some of the figures used in the first manuscript. Finally, I would like to thank

Drs. Robert Harrison, Michael Cowan, Darren Kramer and Reggie Hamdy for their collaborative support in our successful grant applications.

1 Introduction

1.1 Rationale

Despite significant advances in surgery over the last century, most surgical approaches necessitate rather basic cold steel instruments under the control of the surgeon's hand. It has been well documented that scalpels, saws, and drills cause significant tissue trauma through shearing forces, vibrations, or thermal injury [1, 2]. The resultant tissue inflammation is responsible for side effects and complications such as scarring, poor wound, and non-union and failure of osseointegration in osseous tissue [3]. Furthermore, due to their inherent imprecision and human operation, the use of these crude instruments is not without considerable risk of inadvertent tissue injury [4].

Advances in photonics and laser design brought great promise for advancing precision in surgical tissue manipulation. Although proven precise, conventional lasers have since been shown to cause significant tissue injury through thermal and acoustic shockwave effects [5]. As such, their clinical use remains limited to a few specific clinical applications, primarily in the fields of ophthalmology, dermatology, and otorhinolaryngology [6].

More recently, a new generation of pulsed lasers has been engineered. These 'ultrafast' lasers are able to deposit concentrated packets of photons in pulses on the order of trillionths of a second or less [7]. With the capability of depositing energy in a time frame quicker than both the thermal and stress relaxation times of tissue, deleterious thermal and acoustic transient effects on the tissue are negated. A novel ultrafast picosecond infrared laser (PIRL) system has recently been developed [8]. In providing a means to precisely cut both soft and osseous tissue without damaging shearing forces, heat or vibrations, this technology has immense potential in advancing the techniques and

healing outcomes across a vast array of surgical fields. As this technology is currently in its infancy, data confirming its clinical potential is limited. To date, no study has directly measured and confirmed negligible tissue heating during active ablation using the PIRL system. The current study seeks to assess the degree of peripheral tissue heating during PIRL ablation by direct measurement using infrared thermal imaging.

1.2 Objectives and hypothesis

The objective of this research is to measure and compare real-time heating of tissue during ablation of *ex vivo* soft tissue and bone using a PIRL versus conventional microsecond pulsed Er:YAG laser. It is hypothesized that heating as measured by infrared thermography will be significantly lower during soft and hard tissue ablation using a PIRL in comparison to ablation using a microsecond Er:YAG laser. The null hypothesis (N_0) for both cases is that heat generation will be equivalent or greater using a PIRL in comparison to a microsecond Er:YAG laser.

2 Review of relevant literature

2.1 Tissue trauma from conventional surgical instrumentation

Conventional surgical approaches to both soft and densely calcified tissue are associated with significant tissue trauma. The mechanism of soft tissue incision using a surgical scalpel or scissors involves the application of a shearing force to the target tissue until deformation reaches a level sufficient to overcome the ultimate tensile strength (UTS) of the tissue matrix, resulting in fracture and tissue separation [9]. This force, applied in a perpendicular plane relative to the tissue fibers, is distributed over the area of the blade in contact with the tissue. Tissue composition determines what minimal requirement of force per unit area, or pressure, is required for shearing to occur. Once shearing occurs in a tissue, any additional applied cutting force is directed into translational motion of the blade and subsequent shearing of deeper layers. The effects of the applied shearing force are not, however, limited only to the area in contact with blade. As the cutting force is applied, energy disperses radially outward from the contact area. Even sharp surgical scalpel blades, whose cutting edge thickness is typically on the order of 1 μm [10], cause disruption of the extracellular matrix up to 400 μm away [11]. The resultant induced inflammatory response leads to macrophage influx, tumour growth factor (TGF) β signaling, fibroblast proliferation, and excess deposition of collagen leading to scar formation [12]. The search continues for the ideal replacement for the surgical scalpel. Previously reported methods include conventional lasers, ultrasonic devices, and various types of electrocautery [10, 12-17]. Despite significant interest, no novel technology has proven significantly superior to the conventional surgical scalpel in reducing scarring to warrant widespread use. Scarring resulting from surgical incisions remains a significant cosmetic and functional issue across all realms of surgery.

The manipulation of osseous tissues remains an even cruder task in surgery, typically requiring mechanical saws, burrs, and drills. In addition to their inherent imprecision, these instruments generate significant vibrations and thermal damage [1, 2]. Osseous temperatures higher than 100 °C have been recorded during bone removal with mechanical burrs despite the use of a liquid coolant [18]. Heating osseous tissue above 60 °C has been conclusively shown to inactivate alkaline phosphatase, interrupt blood flow, and cause tissue necrosis [1, 19-21] leading to delayed tissue healing. In reconstructive surgery involving osseous free flaps, delayed healing has the potential to lead to disastrous consequences such as fibrous non-union [3]. In osseous drilling for implantation of osseointegrated devices such as dental implants or bone anchored hearing aids (BAHA), thermal damage can lead to failure of osseointegration [22]. Furthermore, mechanical instruments carry significant risk of plunging injuries and collateral damage to adjacent vital soft tissue structures [4]. In regions of dense critical anatomy such as the head and neck, the risk of collateral damage is of particular concern.

2.2 Conventional lasers in surgery

Conventional lasers – what will be defined here as continuous wave (CW) and pulsed lasers with pulse widths on the order of nanoseconds or longer – have been extensively and advantageously used in specific soft tissue applications in otolaryngology, ophthalmology, and dermatology for more than twenty-five years [23]. Some examples of their use include laryngeal tumour surgery, superficial cutaneous skin lesion ablation, refractive corneal shaping, and photo-coagulation of vascular lesions. Although initially promising, conventional lasers have not demonstrated significantly improved scarring outcomes in surgical skin incisions to warrant their general use for this

purpose, primarily due to thermal injury and subsequent significant induction of inflammation in the wound repair process [11, 14]. Furthermore, their use has proven inferior over mechanical instruments where osseous manipulation is required; conventional laser ablation of calcified material is much more time consuming when compared to mechanical means [24] and results in even more heat spread and thermal damage to surrounding tissues [25]. As a result, the use of conventional lasers for manipulation of osseous tissue in surgery has been extremely limited [6]. Recently, a newer generation of 'ultrafast' lasers have been developed [7]. As will be discussed, these lasers interact with tissue in a fundamentally different way than conventional lasers currently in clinical use.

2.3 Basic LASER physics

2.3.1. Properties of LASER light

LASER is an acronym for Light Amplification by Stimulated Emission of Radiation. A laser consists of an excitable medium (solid, liquid, or gas) contained between two mirrors, one which is completely reflective, and one which is partially transmissive. First postulated by Einstein in 1917 [26], the first demonstration of a functional laser in the visible range of light was by Maiman in 1960, using a ruby crystal [27] as the active medium. 'Stimulated emission' is the term given to the emission of a photon from an excited atom when it is stimulated by an incident photon released from a similarly excited atom. The result is a stream of photons that are collimated, monochromatic, and coherent. Collimation is the property by which laser light may travel large distances without beam divergence. Monochromaticity of laser light occurs as a direct consequence of the quantization of energy states within an excited atom or

molecule; stimulated emission within an excited laser medium occurs only for a specific orbital energy level corresponding to a photon of fixed wavelength upon electronic relaxation. Coherence refers to the property by which laser photons travel in phase with each other, another direct consequence of stimulated emission and the wave nature of light; it is this property of laser light which permits for the complex interference patterns required for hologram generation [28].

2.3.2. Radiometric parameters

The duality theory of light that states that electromagnetic radiation exists as both a wave and a particle ('photon'), with a discrete energy defined by

$$Q_{photon} = h\nu, \qquad \text{Eq. 2.1}$$

where Q_{photon} is the energy of the photon (radiant energy) typically expressed in units of electron volts (eV) or Joules (J), h is the Planck constant (4.136×10^{-15} eV·s or 6.626×10^{-34} J·s), and ν is the frequency of the electromagnetic wave in units of cycles per second (s^{-1}). The electron volt is defined by the amount of energy it takes to move a single electron across an electric potential difference of one volt, where

$$1 \text{ eV} = 1.602 \times 10^{-19} \text{ J}. \qquad \text{Eq. 2.2}$$

The frequency and wavelength of an electromagnetic wave are inversely related where

$$\lambda = c/\nu, \qquad \text{Eq. 2.3}$$

where λ is the wavelength of light in units of length (m) and c is the speed of light (3.0×10^{8} m/s in vacuum). Eq. 1 may be rewritten as

$$Q_{photon} = hc/\lambda, \qquad \text{Eq. 2.4}$$

illustrating the inverse relationship between the energy of a photon and its wavelength. It is clear from Equation 2.4 that photons with short wavelengths (eg. ultraviolet, x-, and

gamma-ray) carry more energy than those with longer wavelengths (eg. infrared, micro-, and radio-wave).

In any discussion concerning laser-material interactions, it is necessary to define the parameters of laser power and irradiance. Laser power (*P*), also referred to as radiant power, is the amount of laser energy delivered over time, and is typically defined in units of Watts (Joules per second) using the formula

$$P = \frac{\mathrm{d}Q}{\mathrm{d}t}, \qquad \text{Eq. 2.5}$$

where d*Q* is the amount of radiant energy over a given period d*t*. The radiant energy (d*Q*) emitted by a monochromatic laser over a time period d*t* may be defined by

$$\mathrm{d}Q = N_p \cdot Q_{photon}, \qquad \text{Eq. 2.6}$$

where N_p is the number of photons emitted. Laser irradiance (*I*), also referred to as radiant flux density, is the amount of laser power received per unit of surface area. It is typically defined in units of W/cm^2 using the formula

$$I = \frac{\mathrm{dP}}{\mathrm{d}A}, \qquad \text{Eq. 2.7}$$

where d*A* is the area of interest, most typically the cross-sectional beam diameter at the laser-material interface (usually circular with radius *r* and area πr^2).

Lasers may be operated in different modes. Lasers operating in continuous wave (CW) mode emit an uninterrupted stream of photons, where the emitted power and irradiance remains constant over time. Laser operating in pulsed modes emit concentrated packets of photons, each pulse lasting a time τ_p, interspaced by much longer periods without photon emission. The time profile of the energy rise of each pulse (on an energy plot as a function of time) typically resembles a narrow Gaussian distribution; for pulsed lasers, τ_p is generally determined using the full width at half maximum (FWHM)

of the Gaussian peak. It is possible to define the energy contained in each pulse (Q_p), typically defined in Joules (J), by the formula

$$Q_p = N_p \cdot Q_{photon}, \quad \text{Eq. 2.8}$$

where N_p is the number of photons per pulse. Q_p may be easily measured using commercially available energy meters. Laser fluence (ϕ), also called radiant exposure, describes the amount of laser energy delivered in a laser pulse of time width t_p to a defined surface area. It is typically defined in units of J/cm^2 using the formula

$$\phi = \int_0^{\tau_p} I \mathrm{d}t = \int_0^{\tau_p} \frac{\mathrm{dP}}{\mathrm{d}A} \mathrm{d}t. \quad \text{Eq. 2.9}$$

For a pulsed laser system having a pulse width τ_p, pulse energy Q_p, and a typical circular output beam with a cross-sectional Gaussian energy profile distribution of radius r, calculation of peak fluence (ϕ_p) may be determined by

$$\phi_p = \frac{2Q_p}{\pi r^2}, \quad \text{Eq. 2.10}$$

where a factor of 2 is introduced to account for the peak intensity in the centre of the Gaussian beam. (The other most common beam cross-sectional energy profile is 'flat-top'; in this case, the factor increase of 2 in the peak intensity is dropped). Similarly, the peak irradiance (I_p) for a pulsed laser system emitting a Gaussian beam may be readily determined using

$$I_p = \frac{2Q_p}{\tau_p \cdot \pi r^2}. \quad \text{Eq. 2.11}$$

Peak power (P_p) for such a system becomes

$$P_p = \frac{Q_p}{\tau_p}. \quad \text{Eq. 2.12}$$

For pulsed lasers, it is imperative to differentiate between average power ($\bar{P}$) and peak power (P_p). Average power is determined using the time period between successive pulses (τ_{pp})

$$P_p = \frac{Q_p}{\tau_{pp}}, \qquad \text{Eq. 2.13}$$

where $\tau_{pp} >> \tau_p$, the difference becoming more pronounced the shorter the pulse width. As a result, as demonstrated in Figure 2-1, pulsed lasers may be used to generate peak power several orders of magnitude larger than CW laser systems. It is these peak values that largely govern which type of laser-tissue interaction will occur. Outside of ophthalmology, the majority of lasers in clinical use are limited to pulses on the order of 10^{-3} to 10^{-6} s, capable of modest peak irradiance values. Newly developed 'ultrafast'

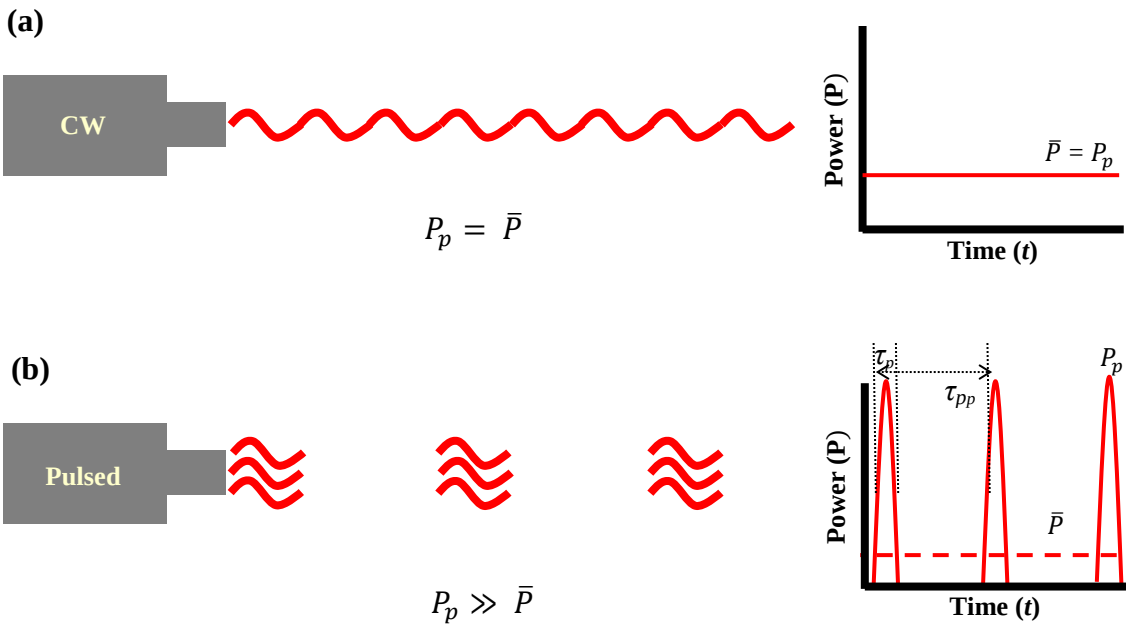

Figure 2-1: Continuous wave versus pulsed laser output modes. **(a)** Continuous wave mode lasers emit a constant stream of photons; power (P) output is constant over time (t), with peak power (P_p) equal to average power ($\bar{P}$) . **(b)** Pulsed mode lasers emit concentrated bundles of photons in short pulses of time (τ_p) interspaced by much longer pulse-to-pulse periods of time (τ_{pp}). As a result, very large values for P_p are possible.

lasers emit pulses with durations of 10^{-12} s (picoseconds) or 10^{-15} s (femtoseconds), and are hence may be used to generate much higher peak irradiance values. As will be discussed, special laser-tissue interactions occur that may be utilized for tissue ablation at such extremes of irradiance [28].

2.4 Mechanisms of laser-tissue interaction

2.4.1. Air-Tissue interface

Light incident on a tissue surface may be reflected, refracted, scattered, transmitted, or absorbed (Figure 2-2). Most commonly, combinations of these occur to varying degrees dependent primarily on the optical properties of the tissue – which fluctuates within any given tissue volume due to inhomogeneity in the distribution of organic, mineral and water content – and the wavelength and intensity of the incident light [28].

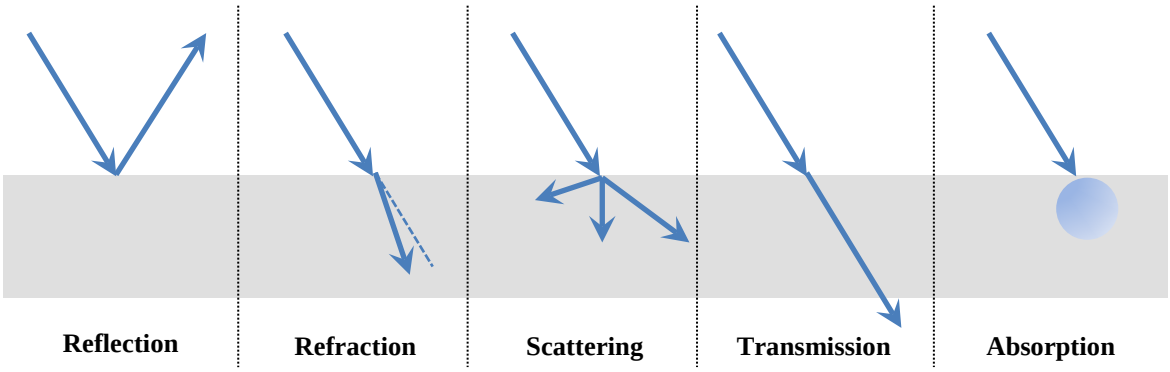

Figure 2-2: Types of light-tissue interactions at the air-tissue interface. Reflection, refraction, scattering, transmission, absorption, or combinations of these may occur.

2.4.2. Photon absorption

Photon absorption is the process through which the intensity of an electromagnetic wave travelling through a given medium is attenuated; and involves photon energy

transfer to the medium's constituent molecules. This energy transfer typically occurs via photon absorption into a molecular vibration or libration mode (visible, infrared and longer wavelengths), absorption into a quantized electronic orbital level (visible, ultraviolet and shorter wavelengths), or by collision with an unbound electron in a process known as inverse Bremsstrahlung absorption. The latter may occur in metals or semiconductors, or within a plasma cloud, causing an increase in the kinetic energy of 'quasi-free' electrons. Absorption of a photon into a quantized electron orbital level (photochemical absorption) leads to elevation of the electron to a higher energy state. If a photon of sufficient energy is absorbed, ionization and/or subsequent photochemical reactions may occur. Otherwise, relaxation of the electron to its initial state usually occurs by either radiative (fluorescence) or non-radiative (heat dissipation) decay [29]. Absorption of lower energy photons into molecular vibration or libration modes (photothermal absorption) leads to a rapid increase in the amplitude of oscillation, followed by relaxation through energy redistribution to the adjacent inter-molecular network as heat [30]. Examples of such intra-molecular vibrations and libration modes are shown in Figure 2-3 for water molecules, each mode corresponding to a particular harmonic vibrational frequency. Of particular note is the asymmetrical stretch mode of the O-H bond, which shows peak vibrational absorption at a frequency of 3400 cm^{-1}, corresponding to a wavelength near 2.94 μm. Note that in vibrational spectroscopy wavelengths are converted into more easily managed wavenumbers, having units of reciprocal centimeters (cm^{-1}). The spectroscopic wavenumber ($\bar{\nu}$) represents the number of wavelengths (or wave cycles) per cm, and is defined by

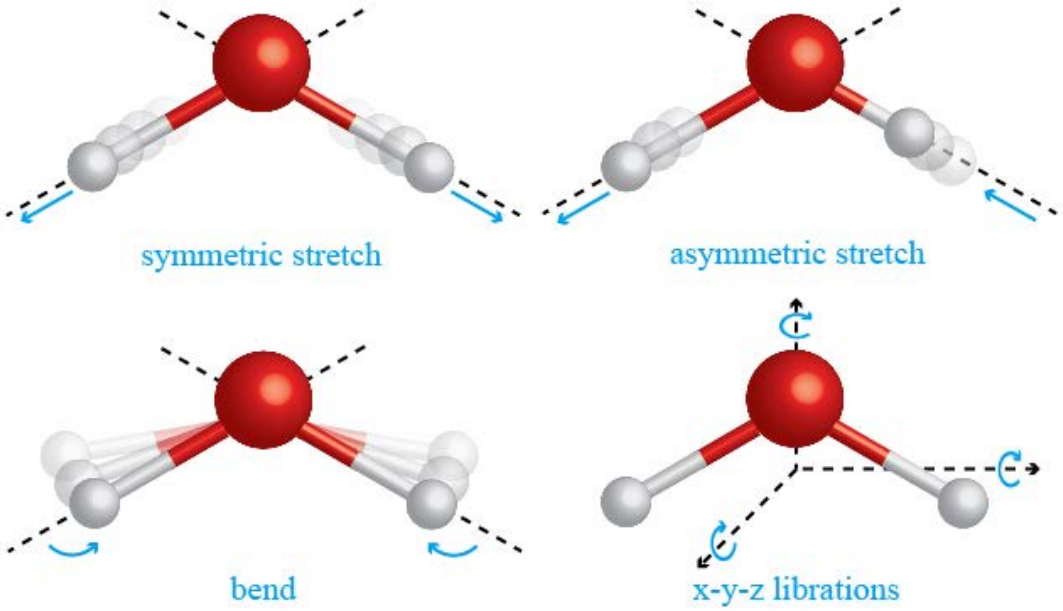

Figure 2-3: Vibrational modes of water molecules. Stretching or bending of the oxygen-hydrogen (O-H) bond or molecular librations in various planes may occur. (Oxygen – red, hydrogen – white).

$$\bar{\nu} = \frac{1}{\lambda}, \qquad \text{Eq. 2.14}$$

where λ is converted to units of cm.

2.4.3. Free radical production and ionization

In the case of tissue, photon induced radical production and ionization is of particular concern, due to its mutagenic potential. Radicals (also called 'free radicals') are highly reactive molecules possessing unbound electrons. Radical production results from chemical bond cleavage, which may occur as a direct consequence of high energy photon absorption, or secondary to extreme temperatures (≥ 1000°C) [31]. Such extreme temperatures are commonly encountered in various forms of laser ablation of tissue, and will be further discussed in a subsequent section. Direct cleavage of organic bonds may be caused by photons having energies greater than 3.5 eV (ultraviolet or shorter wavelengths) by photon absorption into a quantized molecular orbital. Table 2.1 lists

dissociation energies for the most common chemical bonds found in biologic tissue, together with the corresponding photon wavelengths.

Ionization is the liberation of a bound electron from an atom or molecule. Similar to free radical production, ionization may occur as a direct consequence of high energy photon absorption or extreme temperatures in a process known as thermionic emission. Ionization requires significantly more energy, either single photons with energies greater than 10 eV (corresponding wavelengths shorter than 125 nm), or extreme temperatures in excess of several thousand degrees Celcius [32]. Although there currently exist no medical lasers with photon energies greater than 6.4 eV (which corresponds to the 193 nm output of the argon fluoride ArF laser used in ophthalmology), lower energy photon absorption may directly lead to ionization via multiphoton absorption. Multiphoton absorption is the process whereby multiple photons are simultaneously absorbed into an electronic orbital level, acting as a single higher energy photon. It requires extreme irradiance levels; such extremes are possible with ultrafast picosecond and femtosecond laser pulses. For example, irradiance on the order of 10^{11} W/cm^2 is required for multiphoton absorption in water at a fluence of 10 J/cm^2 [33], corresponding to a 100 ps pulse width laser. Nanosecond pulses may also lead to tissue ionization via the generation of confined extreme temperatures, which leads to thermionic emission of an electron. Multiphoton absorption and thermionic emission ionization are the initiating events of plasma mediated ablation, which will be discussed in further detail in section 2.5.1.

Table 2.1: Dissociation energies and corresponding photon wavelengths required for dissociation of common organic chemical bonds (data according to Pauling [34]).

Bond	Dissociation energy (eV)	Corresponding maximum photon wavelength required for photoionization (nm)
C=O	7.1	175
C=C	6.4	194
O-H	4.8	258
C-H	4.3	290
N-H	4.1	302
C-O	3.6	344
C-C	3.6	344

2.4.4. Absorption coefficient and optical penetration depth

The degree of absorption of light by a medium depends on the material properties of the medium (such as the type and concentration of atoms and molecules, as well as the material temperature), in addition to the wavelength and intensity of light. Most materials demonstrate selective absorption; water for example absorbs strongly in the infrared but weakly in the visible region of the electromagnetic spectrum. Any discussion of light-tissue interactions requires definition of the absorption coefficient (μ_a), sometimes called the attenuation coefficient. It is defined according to the Beer-Lambert law, which may be expressed as

$$I(z) = I_o\, e^{-\mu_a z}, \qquad \text{Eq. 2.15}$$

where z denotes the distance along the optical axis from the initial point of light-tissue contact, $I(z)$ is the intensity at a given distance z, and I_o is the incident intensity. Figure 2-4 illustrates absorption coefficients for common tissue constituents at low fluence. In the ultraviolet spectrum, proteins and nucleic acids are the primary tissue absorbers, while in the visible range hemoglobin predominates. A narrow window exists in the near infrared (NIR) region where absorption is weak and light may deeply penetrate tissue. This

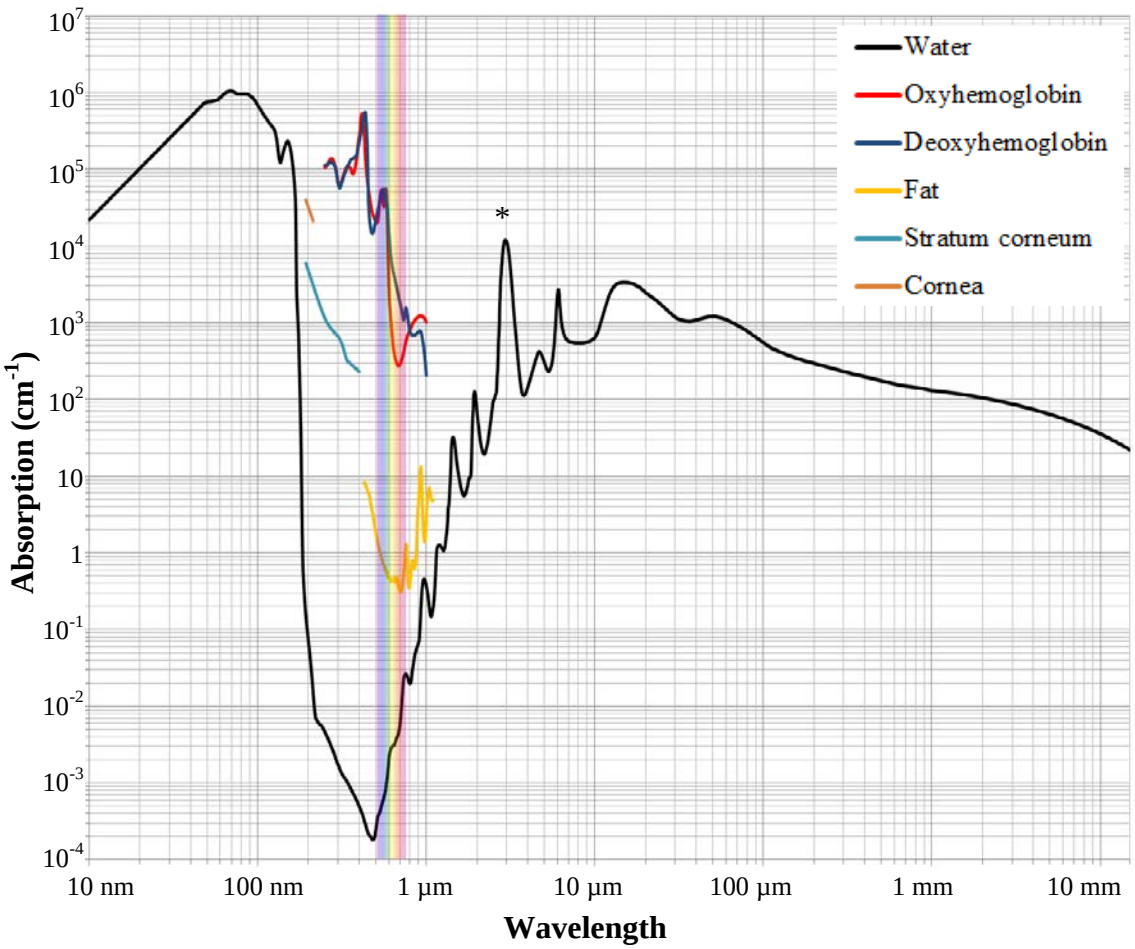

Figure 2-4: Log-log plot of absorption coefficients for various tissue chromophores at nominal fluence levels as a function of wavelength. A peak in absorbance is seen at 2.94 µm for water (*), corresponding to the asymmetric stretch at 3400 cm^{-1}. Data for water from Segelstein and Querry [35], hemoglobin from Prahl and Schenkman [36, 37], fat from van Veen et al. [38], stratum corneum from Prahl [37], and cornea from Pettit and Ediger [39].

'optical window' is often exploited in photodynamic therapy (PDT), where NIR light is used to activate photosensitive chemotherapeutic compounds that have accumulated in tumour cells following exogenous administration [28]. In the mid-infrared region, water governs optical absorption, with a peak absorption seen at 2.94 µm of approximately 12000 cm^{-1} at nominal fluence levels. As described above, this peak corresponds to the asymmetric stretch of the O-H bonds of water molecules. It is important to note however,

the dependence of absorption on light intensity. Above fluence levels on the order of 0.1 J/cm^2, water demonstrates exponentially decreasing absorption. A more detailed description of this phenomenon is beyond the scope of this work; the reader is directed to the excellent review by Vogel et al. [5].

As light propagates through a medium, its energy density at a given location is governed by the optical absorption of the medium and the degree of scattering. In the case where tissue absorption is significantly greater than tissue scattering (which occurs for most wavelengths below 450 nm and above 1.8 μm), it is possible to define the optical penetration depth L (also called the optical absorption length), which corresponds to a given absorption coefficient μ_a [5, 40]. The optical penetration depth is the distance over which the intensity of light incident on a surface has dropped to 1/e, or 37% of its incident value. Using Equation 2.14 with $z = L$, one obtains

$$\frac{I(L)}{I_0} = e^{(-\mu_a L)} = \frac{1}{e}$$

$$L = \frac{1}{\mu_a}. \qquad \text{Eq. 2.16}$$

For example, for a wavelength of 2.94 μm at nominal fluence the optical penetration of water – the primary absorbing constituent of most tissues at this wavelength – is approximately 0.8 μm. It is important to note that at higher fluence levels the penetration depth increases non-linearly due to decreasing absorption.

By multiplying the optical penetration depth L (in cm) with the laser fluence ϕ, one obtains the *volumetric energy density* (in W/cm^2). It is this property (and, more specifically, its rate of change) which principally governs the mechanism of pulsed laser ablation of tissue [5].

2.4.5. Thermal confinement

Another important concept in laser-tissue interactions is that of the time dependent thermal penetration depth Z_{th}, which approximates the rate of vertical heat spread in an absorbing medium, and is given by

$$Z_{th}(t) \approx \sqrt{4\kappa t}, \qquad \text{Eq. 2.17}$$

where κ is the thermal diffusivity of the absorbing medium [28], most commonly water in many laser-tissue interactions where $\kappa = 1.4 \times 10^{-7}$ m^2/s. Figure 2-5 plots thermal penetration (Z_{th}) as a function of time for water. Of note, heat penetrates to a depth of only 0.7 μm within 1 μs in water.

It is possible to define another variable known as the *thermal relaxation time* (τ_{th}) of an absorbing medium by combining the optical penetration depth as given by Equation 2.15 with the thermal penetration depth as given by Equation 2.16 [41]. τ_{th} refers to the

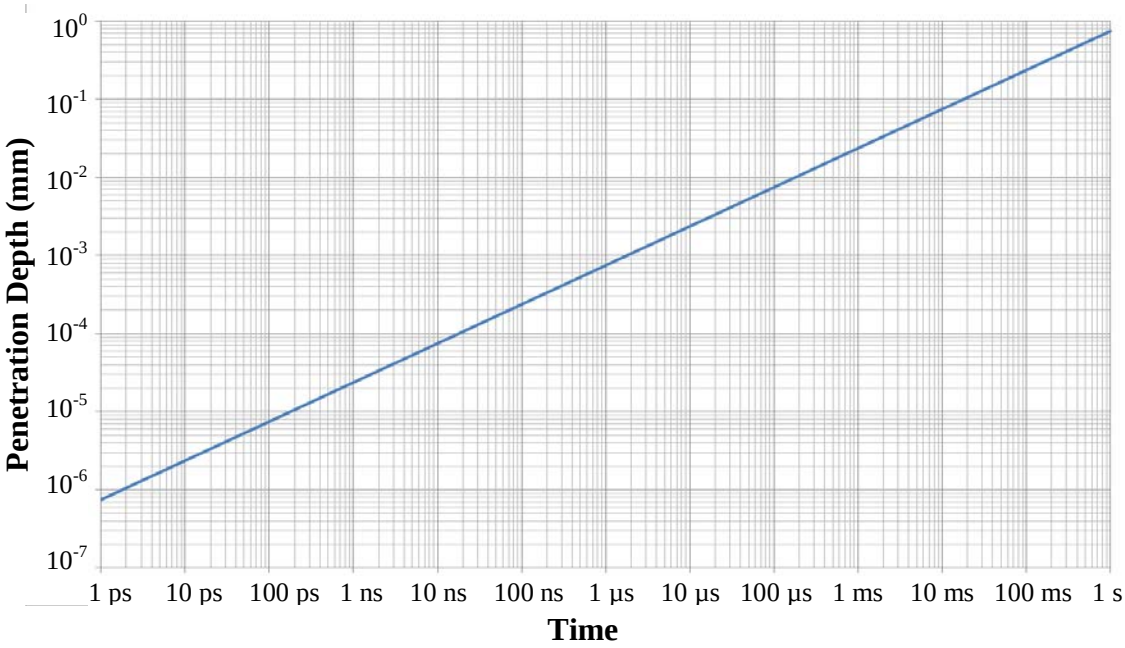

Figure 2-5: Log-log plot of the thermal penetration depth in water versus time.

time required for the thermal energy within the excited target volume to fall to 1/e or 37% of its incident value and is given by

$$\tau_{th} = \frac{{d_{abs}}^2}{4K}, \qquad \text{Eq. 2.18}$$

where d_{abs} either the beam diameter, or the optical penetration depth (L), whichever is smaller [42]. Loss of thermal energy from the target volume occurs due to diffusive collisional energy exchange with the surrounding tissue [30], potentially resulting in thermal injury to the non-ablated region. Such exchange of thermal energy may be largely avoided if material ejection occurs on a more rapid timescale than thermal diffusion. In this case, thermalized photon energy exits the tissue in the form of kinetic energy of the ejected particulate.

It is important to note that τ_{th}, like L, is dependent on the absorbing medium, the wavelength of light being used, and the intensity of the light. The thermal relaxation time is an important concept in pulse d-laser interaction with tissue; if the pulse width τ_p satisfies the condition $\tau_p < \tau_{th,}$ then the criterion for what is called thermal confinement is met. In this situation, all of the pulse energy Q_p is delivered to the tissue before enough time elapses for the energy to begin to diffuse out of the irradiated volume to any significant degree. In the case of tissue ablation, thermal confinement maximizes the temperature rise in the target volume, improving ablation efficiency and minimizing thermal injury to adjacent tissues [42], as discussed above. It is critical to note, however, that even when thermal confinement is met significant adjacent tissue heating may still occur. Such heating is principally dependent on the repetition rate of pulses, the efficiency of the ablation process, and the irradiance level being used. This will be further discussed in a subsequent section. Figure 2-6 demonstrates typical thermal

relaxation times for water as a function of incident wavelength. For example, at a wavelength of 10.6 μm, corresponding to CO_2 laser output, the thermal relaxation time of water (the chief absorbing molecule) is on the order of 700 μs. The shortest thermal relaxation time for water at wavelengths above 190 nm (shorter wavelengths may cause ionization) is approximately 1μs (occurring for wavelengths of 2.94 μm). Hence, where water is the primary chromophore, ablation with lasers having pulse widths < 1μs will always satisfy the requirement for thermal confinement.

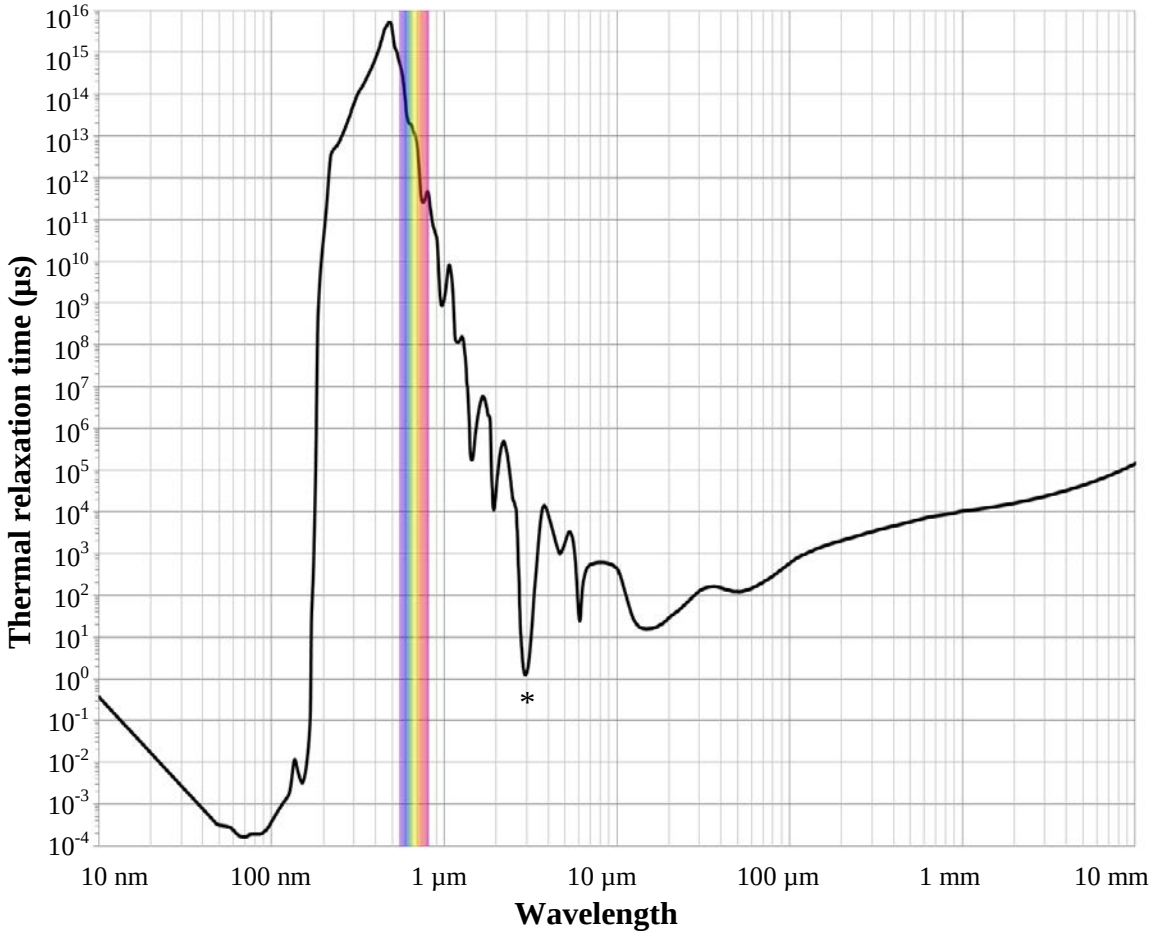

Figure 2-6: Log-log plot of thermal relaxation times for water plotted as a function of wavelength. The shortest relaxation time for non-ionizing wavelengths is 1 μs (*), and occurs at 2.94 μm.

2.4.6. Thermoelastic stress confinement

Short-pulsed laser irradiation of tissue results in rapid heating of a confined volume, which generates considerable thermoelastic stress. This stress quickly leads to volume expansion and the subsequent formation of acoustic transients that propagate away from the target volume, in a fashion similar to, yet distinct from thermal spread [42, 43] . These acoustic transients – typically in the MHz range for nanosecond or longer pulse widths – may lead to significant mechanical injury to distant tissues [8]. As will be discussed, they may also play an important role in tissue ablation.

In a fashion similar to the attainment of thermal confinement in short-pulse laser-tissue interactions, it is possible to define a condition where all the pulse energy *Qp* is deposited in the tissue before enough time elapses for volume expansion, limiting the spread of thermoelastic energy out of the target volume. This condition is known as *stress* or *inertial confinement*, and occurs when the pulse width is shorter than the characteristic acoustic relaxation time τ_{ac}, which is given by

$$\tau_{ac} = \frac{d_{abs}}{v_s}, \qquad \text{Eq. 2.19}$$

where d_{abs} is as above, and v_s is the speed of sound in the tissue [42]. In addition to its variation with v_s, τ_{ac} varies with the wavelength dependent absorption coefficient, which itself varies with the intensity of light. τ_{ac} is several orders of magnitude smaller than $\tau_{th.}$ At nominal fluence levels (under 0.1 J/cm^2), τ_{ac} is approximately 500 ps in soft tissues (calculated using the speed of sound in water at ~1500 m/s) and 200 ps in densely calcified tissues such as bone (calculated using the speed of sound in bone of ~3800 m/s). At higher fluence levels (such as those typically required for tissue ablation) the condition for stress confinement is typically satisfied when $\tau_p < 1$ ns, due to the non-linearity of

absorption at higher fluence as discussed above [8]. In addition to thermoelastic stress, short-pulse laser irradiation of tissue may produce shock waves and acoustic transients through other mechanisms, which include plasma cloud expansion and cavitation. These mechanisms and their implications on tissue ablation will be discussed in the following sections.

2.5 Mechanisms of pulsed laser ablation of tissue

2.5.1. Primary ablation mechanisms

Laser ablation is the creation of a tissue cavity or incision via removal of tissue by photothermal, photochemical, plasma-mediated or photomechanical means. Ablation requires the breakage of intermolecular or intramolecular bonds, which is accomplished via vaporization, molecular fragmentation, or void formation. Distinct primary and secondary ablation mechanisms exist, which, in addition to the target tissue, are chiefly governed by the photon energy (wavelength), pulse width (τ_p), and irradiance (I) used. These variables also determine the pathway of photon absorption into vibrational, electronic, or optical breakdown states. Ablation mechanisms commonly overlap and are often synergistic.

Photothermal ablation is the process whereby photon absorption into vibrational states leads to thermalization causing vaporization and material removal. Primary photothermal ablation is achieved using infrared and visible photons, with the most common primary tissue chromophore being water or hemoglobin respectively. Vaporization may occur through normal boiling, confined boiling, or phase explosion [5]; each forms involves vapor bubble nucleation and growth. The type of vaporization that occurs depends principally on the rate of volumetric energy density (W/cm^3) deposition in

the tissue, which is a function of the optical absorption length (*L*) and the irradiance (*I*). Normal boiling is the process where the absorbing chromophore is heated to its boiling temperature (i.e. 100℃ for water at atmospheric pressure), where it then undergoes a phase change to the gaseous state through vapor bubble growth. A relatively slow process, normal boiling is one of the principle mechanisms for photothermal ablation of tissue using long pulse and CW lasers. As heat is not confined to the target volume during irradiation, significant amounts of total energy are required to drive the ablation process. Heat spread away from the target volume is significant, leading to significant thermal injury to surrounding tissue (although in surgery this may be of benefit in terms of coagulation effects). Confined boiling is the process whereby the absorbing chromophore is heated to temperatures above the standard atmospheric boiling point due to mechanical constraint of the surrounding extracellular matrix (ECM) [5, 44, 45]. Superheating occurs as a result of the increased vapor bubble pressure necessary to overcome the tensile strain of the ECM. Once pressure buildup is sufficient to overcome the ultimate tensile strength (UTS), explosive material ejection occurs. However, if the critical pressure threshold for overcoming the UTS is not reached – the ablation threshold – thermal relaxation occurs with heat distribution away from the target volume. Confined boiling plays a pivotal role in photothermal ablation mechanisms for CW and long pulse lasers, as well as short pulse (i.e. microsecond and nanosecond) lasers [46]. The degree of thermal injury to adjacent tissue depends principally on the rate of energy deposition (i.e. the pulse width), with longer pulses resulting in slower temperature rises and subsequently increased heat spread away from the target volume during ablation. Phase explosions occur when the rate of energy deposition into a tissue chromophore exceeds the rate of vapor bubble growth leading to normal boiling. The chromophore undergoes

superheating, until it becomes unstable at a point known at the spinodal temperature. At this point a phase explosion ensues if pressure buildup is sufficient to overcome the UTS of the surrounding ECM, with ejection of mixed phase vapor and liquid droplets. If the pressure is not sufficient to overcome the UTS, the process continues along the same pathway as confined boiling. Examples of common lasers in clinical use that ablate primarily by photothermal means include the carbon dioxide (CO_2), potassium titanyl phosphate (KTP), and yttrium aluminum garnet (YAG) family of lasers.

Photochemical ablation involves photon absorption into quantized electronic states leading to intramolecular bond fracture and molecular fragmentation. In 1982, it was first noted that nanosecond pulses of far ultraviolet light (meeting conditions for thermal confinement) could result in precision etching of polymer surfaces without collateral thermal or mechanical injury [47, 48]. This observation quickly led to the use of nanosecond argon fluoride (ArF) lasers – called excimer lasers – in corneal refractive surgery. It has been hypothesized that the underlying mechanism involves molecular fragmentation that leads to volume expansion, pressure rise, and subsequent material ejection in a process known as *ablative photochemical decomposition* [5, 47, 49, 50]. Subsequently, it is currently generally accepted that there is always some degree of secondary photothermal effects that occur as a result of electronic relaxation that also serve to drive ablation in excimer surgery [5, 51]. Due to the mutagenic potential associated with free radical production in photochemical decomposition, clinical use of photochemical ablation outside of corneal surgery (where no dividing cells are present) is limited.

Plasma-mediated ablation is the process by which large laser irradiance or fluence levels lead to ionization of tissue and the subsequent generation of a plasma cloud.

Plasma may be generated by thermionic emission using high fluence nanosecond pulses, or by multiphoton absorption using high irradiance picosecond or femtosecond pulses. A fluence on the order of 100 J/cm^2 for a 10 ns pulse with corresponding irradiance on the order of 10^{10} W/cm^2 is required for thermionic emission in water, whereby a fluence of only 1 J/cm^2 will generate a plasma cloud initiated by multiphoton absorption ionization at an irradiance of 10^{13} W/cm^2 for a 100 fs pulse [33, 52]. Electrons liberated via thermionic emission or multiphoton absorption then proceed to continue to absorb photons via inverse Bremsstrahlung absorption, gaining kinetic energy, leading to high energy collisions with neighboring bound electrons, subsequently triggering their release from the bound state (called *impact ionization).* Consequently, photon absorption by the increasing numbers of these quasi-free electrons leads to a cascade of impact ionizations, known as *avalanche ionization*. This leads to the rapid generation of an intensely hot electron dense plasma cloud, which absorbs nearly all incoming light, regardless of wavelength, causing normally transparent materials to be opaque. This phenomenon is known as *optical breakdown* [5, 29, 53-55].

Plasma-mediated ablation is efficient and precise, but is unsuitable for manipulation of regenerative tissues. Plasma-driven ablation has proven effective for metals [56-58] and non-metals [53, 57, 59], including densely calcified tissue such as bone [59-61]. No thermal damage occurs as plasma-mediated ablation necessitates pulse widths on the order of a few nanoseconds or less, hence conditions for thermal confinement are always met. However, live animal experiments have demonstrated severely impaired tissue healing following ultrafast cuts in comparison to standard surgical techniques [61], almost certainly the result of the significant photomechanical phenomena triggered by the formation of a plasma cloud. These plasma-mediated

mechanical effects, which include cavitation and subsequent shock wave and jet production, are collectively referred to as *photodisruption*, and will be discussed in more detail below. In addition to injurious mechanical effects, plasma driven ablation necessitates highly ionizing irradiance; such irradiance levels have been shown to result in the creation of highly reactive oxygen species capable of causing double strand DNA breaks, that may result in mutagenesis or apoptotic cellular death [62]. As a result, the use of plasma-mediated laser ablation where dividing cells are present is unlikely to occur.

2.5.2. Secondary mechanisms and photomechanical ablation

Thermally-induced mechanical weakening of the ECM is an important secondary mechanism in material removal in primary photothermal ablation. Weakening of the ECM occurs secondary to thermally-induced denaturation of ECM structural proteins, reducing the UTS hence permitting for more enhanced material ejection. Thermal weakening plays an especially important role where significant thermal spread away from the target volume occurs. Where conditions for thermal confinement are met (typically requiring nanosecond or shorter pulse widths), superheating of the target volume to temperatures in excess of 1000℃ may occur, resulting in ECM weakening secondary to protein dissociation into volatile fragments. This process is known as photothermal decomposition [31].

Organic gas formation may enhance material removal in primary photochemical, plasma-mediated, and photothermal ablation where photothermal decomposition occurs. Various organic gaseous compounds may be produced from highly volatile free radicals,

molecular fragments, and ionized molecules that result from such methods of ablation. Once formed, these gases rapidly expand, enhancing material ejection [5, 63, 64].

Photomechanical disruption (photodisruption) plays a critical role in precision material removal in plasma-mediated ablation. The formation of plasma within tissue creates a bubble (called a cavitation), filled with rapidly expanding hot plasma ions and vapor. Confined by the surrounding tissue, this cavitation bubble quickly expands, then collapses and ruptures due to the hydrostatic pressure of the surrounding tissue matrix, forming a jet which is always oriented towards the more rigid tissue boundary. The high pressure jet results in precision mechanical ejection of tissue, without thermal injury [65]. Photodisruption is always associated with significant undesirable mechanical effects, however. The rapid expansion at the onset of plasma cavitation bubble formation and the rapid collapse at the termination into a jet triggers high intensity shock waves, which quickly slow to match the speed of sound in the material, forming acoustic transients. These broadband transients are typically in the MHz range for nanosecond pulses and in the GHz range for picosecond or faster pulses. Stress waves in the MHz range are poorly attenuated and hence propagate far away from the target volume, which may lead to significant collateral cellular injury [5, 66] [65]. Despite high precision cuts with no sign of thermal cellular injury, experiments with plasma-mediated ablation in live tissue have demonstrated extremely poor healing outcomes, almost certainly the result of irreversible shock wave induced mechanical cellular injury [61]. The contribution of photomechanical effects to material removal in plasma-mediated ablation cannot be understated. The transduction of photon energy into mechanical energy in the form of shock waves and cavitation bubbles has been estimated to be as high as 90% [5, 33].

Material removal in photothermal ablation may mimic plasma-mediated photodisruptive mechanisms under special conditions. A common scenario is when a layer of liquid water exists between the tissue surface and the fiber tip of a pulsed infrared laser, where the rate of volumetric energy density deposition is high enough such that bubble nucleation by phase explosion may occur. In this instance, the cavitation bubbles are filled with mixed phase liquid water and vapor. In the region of the fiber tip, the expanding bubble is confined, leading to its subsequent collapse and jet formation towards the tissue directly opposite the fiber tip, leading to material removal [67-69] . This is the underlying mechanism behind ablation of teeth using commercially available microsecond pulsed Er:YAG lasers with water spray. The water spray thus serves to cool the underlying tissue as well as serve as the vehicle for ablation, allowing for precision ablation of teeth with minimal thermal injury [70]. Ablation of bone using Er:YAG laser has demonstrated inferior healing outcomes in comparison with conventional surgical instruments [71]. Despite the precision and minimal thermal injury, use of Er:YAG lasers in otologic surgery is limited, as bubble expansion and collapse generate high intensity broadband acoustic transients (including frequencies audible to the human ear), that have been shown to cause threshold shifts in human hearing [72-76].

Short-pulse laser irradiation of tissue leads to the generation of significant thermoelastic stress, which triggers acoustic transients that may enhance material ejection in all forms of primary ablation. Thermoelastic stress is the result of rapid heating and thermal expansion of a confined volume [77]. Initially compressive, the resultant stress waves become tensile following impedance mismatch induced reflection at the air-tissue interface [42]. These tensile waves serve to enhance material ablation in two ways. First, a profound transient reduction in local pressure within the material allows for bubble

formation and expansion at temperatures far below the normal boiling point of the absorbing chromophore [67]. Second, when of sufficient magnitude, these tensile waves may directly induce cavitation and subsequent collapse and jet formation, which overcomes the UTS of the material and results directly in tissue fracture and material ejection [43]. The latter mechanism, first reported by Dingus and Scammon [43], is known as *front surface spallation*. Under conditions of thermal and stress confinement, the energy required to ablate tissue by photomechanical thermoelastic stress waves can be orders of magnitude less than what would be required to remove it through vaporization [42, 78, 79]. Consequently, it was believed that material ejection purely by photomechanical thermoelastic stress waves was theoretically possible [80]. However, initial attempts at material ablation using infrared pulses below potentially mutagenic irradiance and fluence levels either proved inefficient or required temperatures over 200℃ [81, 82]. The conversion efficiency of photon energy to acoustic energy in water was found to be on the order of 10% or less [42, 83]; consequently, the energy required to generate high enough stress waves to cause material fracture always involves levels high enough to trigger other ablation mechanisms [8]. Thus, it is generally accepted that material removal by pulsed laser ablation cannot be achieved using the front surface spallation method alone [5]. More recently, a novel method of pulsed infrared laser irradiation has been found to produce highly efficient material removal by harnessing photomechanical thermoelastic stress effect through a mechanism known as i*mpulsive heat deposition through vibrational excitations* (IHDVE) [8, 30].

Finally, material ejection from a tissue surface generates recoil stress that transfers momentum to the remaining tissue bed. The amount of recoil-associated momentum increases with fluence levels and follows the law of momentum conservation; at high

enough levels, such recoil may induce a secondary expulsion stage, which significantly enhances the rate of material removal in all forms of laser tissue ablation [5, 84]. Importantly, for ablation using pulse lengths in the nanosecond and sub-nanosecond range, such recoil effects are in fact responsible for the bulk of material ejection [5, 30].

2.5.3. Effects of thermal and stress confinement

Use of pulse widths that satisfy thermal and stress confinement conditions enhances material removal while reducing the amount of total energy required for ablation. Consequently, collateral tissue damage is reduced as the degree of both thermal and mechanical injury scale with the total amount of deposited energy [42]. Thermal confinement conditions allow for a higher rate of heat deposition and higher temperature attainment within the target volume, triggering vaporization and material ejection before significant thermal spread occurs. Similarly, stress confinement conditions allow for the generation of higher intensity thermoelastic waves within the target volume, enhancing material fracture and ejection while reducing the spread of potentially mechanically injurious acoustic transients into adjacent tissue. As previously stated, where water is the primary chromophore, thermal confinement is obtained for pulse widths on the order of 1 μs or less whereas both thermal and stress confinement is obtained for pulse widths shorter than 1 ns.

2.5.4. Ablation threshold

The threshold fluence in laser-tissue ablation refers to the fluence level below which the absorbed laser energy does not result in any significant material ejection. The threshold fluence is tissue and laser specific; it is principally dependent on the rate of volumetric energy density deposition and the mechanical properties of the tissue.

Material ejection is required to remove the deposited photon energy from the tissue [5]. When tissue is irradiated below threshold fluence, photon energy is principally thermalized, which may result in significant thermal injury, regardless of whether conditions for thermal confinement are met or not. It is important to note that cross-sectional beam fluence is often non-uniform. For a circular Gaussian beam profile – one of the most common types – the fluence level in the centre of the beam is generally twice as high as that of the periphery. This may result in ablation of tissue in the central path of the beam with heating occurring in the tissue irradiated with the more radial portions of the beam.

2.5.5. Attempts at 'cold' photothermal ablation

The introduction of short pulse microsecond and Q-switched nanosecond Er:YAG lasers brought the hope of achieving a long sought after safe method of 'cold' tissue ablation. These laser systems, which emit photons corresponding to the peak in water vibrational absorption at 2.94 μm, ablate tissue by a photothermal mechanism if no water spray is used, or by a combination of photothermal and photomechanical cavitation and subsequent jet formation if an intervening water layer is used over the tissue (as described in the previous section). With nanosecond pulse widths meeting conditions for thermal confinement, or with microsecond pulses utilizing the photomechanical effect of water cavitation (together with the cooling properties of the water spray), the prospect of precise tissue ablation without the use of free-radical producing wavelengths or significant thermal tissue injury appeared possible. However, healing studies using these pulsed laser systems proved disappointing [8, 11, 71, 85, 86]. As neither microsecond nor nanosecond pulsed Er:YAG lasers meet conditions required for acoustic stress

confinement, significant energy loss out of the target ablation volume occurs in the form of acoustic transients. These transients are typically in the MHz range, and readily propagate through tissue leading to widespread mechanical injury to bordering cells and subsequent impaired wound healing [8]. In addition to mechanical injury, complete thermal confinement is not possible, and significant thermal injury still occurs [8, 11, 86-88]. Studies have confirmed thermal necrosis with microsecond Er:YAG laser ablation at fluence levels typical for use in clinical practice [8, 11, 86]. Furthermore, loss of energy out of the target volume through thermalization and mechanical acoustic transients leads to higher total energy requirements for material ejection. A microsecond Er:YAG laser has an ablation threshold fluence on the order of 1.5 J/cm^2 for human skin, which, as will be discussed, is significantly higher than threshold for ablation using a more efficient and novel infrared picosecond laser.

2.5.6. IHDVE (*I*mpulsive *H*eat *D*eposition through *V*ibrational *E*xcitations)

With the advent of the ultrafast pulsed picosecond infrared laser (PIRL), a novel method of efficient photomechanical laser ablation was realized. The PIRL emits photons at 2.94 μm, similar to Er:YAG lasers, albeit in picosecond time scales that meet conditions for both thermal and acoustic stress confinement. As discussed, photons having a 2.94 μm wavelength are strongly absorbed by the asymmetric stretch vibrational mode of the O-H bond of water at 3400 cm^{-1}. Cowan et al. demonstrated that complete thermalization of vibrational energy absorbed into intramolecular O-H bonds at 3400 cm^{-1} into the intermolecular H-bond network occurs within 1 ps [89]. The properties of water that enable it to strongly absorb at 2.94 μm and subsequently completely thermalize the absorbed energy on an ultrafast picosecond timescale allow for the impulsive

superheating of water capable of driving rapid phase transitions [30]. Use of pulse widths between ten and a few hundred picoseconds – shorter than both the thermal and acoustic stress relaxation times of water – maximizes energy confinement to the target volume. Such picosecond pulse widths also allow for complete thermalization to occur in step with the rate of photon deposition; the use of shorter pulse widths (shorter than the aforementioned thermalization time) may result in vibrational ladder climbing or multiphoton absorption, leading to free radical production or ionization [30]. The use of infrared picosecond pulses in this manner has been coined *impulsive heat deposition through vibrational excitations* (IHDVE) [8].

Material removal using IHDVE ablation occurs primarily through phase explosions, greatly enhanced by thermoelastic photomechanical effects. The picosecond timeframe results in rapid superheating leading to phase explosions and the subsequent generation of powerful thermoelastic stress transients in the GHz range [83]. Such GHz transients are significantly attenuated over a distance similar to the optical penetration depth, minimizing the risk of mechanical injury to cells outside of the target ablation volume [8]. Importantly, confinement of the GHz transients to the ablation volume leads to powerful stress amplitudes on the order of 1 GPa for fluence levels on the order of 1 J/cm^2 in pure water [8]. The thermoelastic photomechanical effect is thus significantly enhanced, catalyzing the phase explosions of the superheated water while also causing direct material fracture and ejection. Table 2.2 summarizes ablation mechanisms for several common types of medical laser systems and their respective potential for tissue injury.

Table 2.2: Comparison of ablation mechanisms and the potential for tissue injury among selected medical laser systems and the PIRL.

Pulsed laser system	**λ**	**τ_p**	**Common clinical application**	**Primary Chromophore**	**Ablation Mechanisms**		**Mutagenic potential**	**Potential for tissue injury**	
					Primary	**Secondary**		**Thermal**	**Mechanical**
KTP	532 nm	ms	Vessel coagulation	Hemoglobin	Photothermal (vaporization via normal +/- confined boiling)	Thermal weakening of ECM	No	++++	-
CO2	10.6 μm	ms	Ablative surgery (e.g. laryngeal mass)	Water	Photothermal (vaporization via normal +/- confined boiling)	Thermal weakening of ECM	No	++++	-
Super/ultrapulse CO2	10.6 μm	μs	Skin resurfacing	Water	Photothermal (vaporization via confined boiling and phase explosions)	Thermal weakening of ECM, recoil	No	++	++
Er:YAG	2.94 μm	μs	Dental surgery	Water	Photothermal (vaporization via confined boiling and phase explosions)	Thermal weakening of ECM , cavitation and jet formation with intervening water layer, recoil	No	++ (reduced with water spray)	++
PIRL	2.94 μm	ps	Tissue incision (*proposed*)	Water	Photothermal (vaporization via phase explosions)	Photomechanical thermoelastic stress, recoil	No	-	-
ArF	193 nm	ns	Corneal refractive surgery	Collagen	Photochemical (ablative photodecomposition)	Photothermal decomposition of ECM, gas formation, recoil	Yes	-	++
Femto-second	1052 nm	fs	Capsulorrhexis	Any (optical breakdown)	Plasma-mediated	Photodisruption, recoil	Yes	-	+++

2.5.7. Preliminary studies with a novel picosecond infrared laser system

A novel picosecond infrared laser system, or PIRL, that utilizes IHDVE ablation has recently been developed and tested [8]. In the first reported study examining PIRL ablation of *ex vivo* healthy tooth enamel, no thermal injury or micro-fracture was seen using scanning electron microscopy [8]. The minimal fluence necessary for ablation for the PIRL was determined to be on the order of 0.5 J/cm^2 for densely calcified tissue [8], less than half that required for microsecond Er:YAG laser ablation of soft tissue.

Direct comparison of wound healing responses following PIRL ablation versus conventional surgical laser and surgical scalpel has shown impressive results. In a preliminary wound healing experiment by Amini-Nik et al.[11], full thickness incisional and excisional soft tissue wounds were generated in CD1 mice using PIRL, a conventional surgical laser (Er:YAG), or conventional scalpel. Transmission and scanning electron microscopy showed that the PIRL laser produced precise tissue cuts with less damage to surrounding tissues than wounds created using the other modalities. The width of the scars formed by PIRL incision were half that of those produced using either Er:YAG laser or scalpel. Aniline blue staining showed higher levels of collagen in the early stage of the wounds produced using the PIRL laser, suggesting that these wounds mature faster. There were more viable cells extracted from skin using the PIRL laser, suggesting less cellular damage. Beta-catenin and TGF-β signaling, (which are activated during the proliferative phase of wound healing, and whose level of activation correlates with the size of wounds), was lower in wounds generated by the PIRL system. In addition, wounds created with the PIRL system showed a lower rate of cellular proliferation.

Experimentation with the PIRL system is still in its infancy. Fundamental characteristics such as the optimum beam shape profile, energy setting, and pulse repetition rate to obtain maximal ablation efficiency without deleterious effects have yet to be determined. Importantly, whether any heat is generated during active PIRL ablation of tissue is still unknown.

2.5.8. Measurement of temperature rise during laser ablation

Thermography involves the use of quantitative digital imaging to determine temperature. It is based on the principle of blackbody radiation, whereby any opaque and non-reflective body (blackbody) will emit a characteristic electromagnetic radiation spectrum dependent only on its temperature [90]. As the emitted spectrum lies primarily in the infrared region of the electromagnetic spectrum, infrared cameras are typically used for thermal imaging. A thermal imaging system consists of an infrared photo-detector coupled to a computer with software capable of integrating the emitted spectral pattern from the material surface under investigation in order to generate temperature data points for each detector pixel.

Quantitative monitoring of tissue temperature rise during ablation is important in the testing phase of any new medical laser system. Firstly, as no photothermal ablation method occurs in a completely adiabatic fashion, the risk of significant heat accumulation due to inefficient material ejection or beam shape effects (as discussed in section 2.5.4) always exists. Temperature measurement during ablation is important, as cellular injury resulting from thermal denaturation of enzymes in the absence of histologically evident necrosis may occur for temperature rises as low as 18°C above normal [45, 91-93]. Secondly, temperature rise in adjacent tissue may be considered an inverse surrogate

marker for the energy efficiency of an ablation mechanism. Energy lost to the material removal process is primarily thermalized, leading to temperature rises in the remaining tissue. Infrared thermography provides an accurate, reproducible, and non-contact method of measuring tissue temperature rises during laser ablation; it has been extensively used to study laser-induced temperature changes in various materials, including tissue [94-100].

2.5.9. Linking statement to first manuscript

As the PIRL technology is still in its infancy, there is a paucity of data demonstrating its cold ablation capability in practice. The following manuscript is a study that directly compares heat generation during superficial ablation of *ex vivo* porcine skin using both the PIRL and microsecond Er:YAG laser by means of thermography. It is the first study to directly measure heat generation in real-time during ablation using the PIRL.

3 Manuscript 1 – Heat generation during ablation of porcine skin with Er:YAG laser versus a novel picosecond infrared laser (PIRL)

(Currently in press – *JAMA Otolaryngology – Head and Neck Surgery)*

Submitted: Oct 23, 2012

Revisions submitted: Nov 22, 2012

Accepted for publication: Dec 19, 2012

Nathan Jowett MD FRCSC[1,2*], Wolfgang Wöllmer PhD[2*], Alex M. Mlynarek MD MSc FRCSC[1], Paul Wiseman PhD[3], Bernard Segal PhD[1], Kresimir Franjic PhD[4], Peter Krötz MSc[4], Arne Böttcher MD[2], Rainald Knecht MD PhD[2], RJ Dwayne Miller PhD[4]

[1]Department of Otolaryngology – Head and Neck Surgery, McGill University, Montreal, Canada

[2]Department of Oto-, Rhino-, Laryngology, University Medical Centre Hamburg-Eppendorf, Hamburg, Germany

[3]Departments of Chemistry and Physics, McGill University, Quebec, Canada

[4]Atomically Resolved Dynamics Division, Max Planck Research Department for Structural Dynamics, University of Hamburg, Hamburg, Germany

*Author to whom correspondence should be addressed:

1. Dr. Nathan Jowett

Department of Otolaryngology – Head and Neck Surgery

Jewish General Hospital

3755 ch. de la Côte-Sainte-Catherine, Suite E-903

Montréal, QC, Canada H3T 1E2

Telephone: +1 514 340 8222 x8246, Fax: +1 514 340 7934

E-mail: nathan.jowett@mail.mcgill.ca

Article Type: Original Article

Section/Category: Reports of basic science

3.1 Abstract

Background: Lasers provide a means of precise surgical ablation, but their clinical use has remained limited due to undesired thermal, ionizing, or acoustic stress effects leading to tissue injury. A novel ultrafast, non-ionizing, picosecond infrared laser (PIRL) system has recently been developed and is capable, in theory, of ablation with negligible thermal or acoustic stress effects.

Objective: The purpose of this study was to measure and compare heat generation by means of thermography during ablation of *ex vivo* porcine skin by conventional microsecond pulsed Er:YAG laser and PIRL.

Methods: *Ex vivo* porcine skin was ablated in a 5mm line pattern with both Er:YAG laser and PIRL at fluence levels marginally above ablation threshold (2 J/cm^2 and 0.6 J/cm^2 respectively). Peaks and maxima of skin temperature rises were determined using a thermo camera. Means of peak temperature rises were compared using paired sample t-test. Ablation craters were assessed by means of digital microscopy.

Results: Mean peak rise in skin surface temperature for the Er:YAG laser and PIRL was 15.0°C and 1.68°C, respectively ($p < 0.001$). Maximum peak rise in skin surface temperature was 18.85°C for the Er:YAG laser and 2.05°C for the PIRL. Ablation craters were confirmed on digital microscopy.

Conclusions: PIRL ablation results in negligible heat generation, considerably less than Er:YAG laser ablation.

Keywords: laser ablation, cold ablation, picosecond infrared laser, Er:YAG laser

3.2 Introduction

Despite significant advances in surgery over the last century, most surgical instrumentation remains basic. It has been well documented that conventional instruments, such as scalpels, saws, and drills cause significant tissue trauma through shearing forces, vibrations, or thermal injury [9, 11, 12]. Furthermore, due to their inherent imprecision and human operation, use of these crude instruments is not without considerable risk of inadvertent tissue injury. Advances in photonics and laser design have brought great promise for advancing precision in surgical tissue manipulation. Although they offer precision, conventional lasers have since been shown to cause significant tissue injury through combinations of ionizing, thermal, or acoustic shockwave effects [5, 8, 11]. As such, their clinical use remains limited [6].

The introduction of non-ionizing, short pulse microsecond (10^{-6} seconds) and Q-switched nanosecond (10^{-9} seconds) Er:YAG lasers brought hope of achieving a long desired means of 'cold' laser ablation. With shorter pulses, photomechanical ablation is possible, when the absorption of a laser pulse in the target tissue creates mechanical stress leading to material fracture and ejection [42]. Since tissue has a thermal relaxation time on the order of a few microseconds [101], the ability to remove it without significant thermal injury using short pulses seemed possible, in theory [8, 11, 71, 85, 86]. As relatively high fluence (defined as the amount of light energy incident on a given square area) levels are required for Er:YAG laser ablation, (at > 1.5 J/cm^2), complete thermal confinement is not possible, and significant thermal injury still occurs due to temperature superposition [8, 11, 86-88]. Studies have confirmed thermal necrosis with Er:YAG laser ablation at fluence levels common in clinical practice [8, 11, 86]. As irreversible thermal denaturation of human proteins is known to occur at short exposures to temperatures as

low as 18°C above body temperature, cellular injury is possible even in the absence of immediately obvious histologic necrosis [45, 91-93]. Furthermore, as a result of acoustic stress relaxation times being on the order of 1 nanosecond for human tissue, even microsecond and Q-switched nanosecond Er:YAG laser pulses result in propagation of acoustic transients which lead to distant fracture of the extracellular matrix, increasing inflammation [8].

Recently, a new generation of 'ultrafast' lasers has been developed [7]. These 'ultrafast' lasers deposit concentrated pulses of photons on a picosecond (10^{-12}) time scale or less, shorter than both the thermal and stress relaxation times of tissue. As such, deleterious thermal and acoustic shockwave effects are negated [8].

A novel, non-ionizing ultrafast picosecond infrared laser (PIRL) system has recently been developed that is capable, in theory, of true 'cold' photomechanical ablation [8]. As this technology is currently in its infancy, data confirming its clinical potential is limited. Previous wound healing studies by Amini-Nik et al. has shown zones of injury significantly smaller on scanning electron microscopy for full thickness incisions made by PIRL when compared with scalpel and Er:YAG laser [11]. In addition, the width of the scars formed by PIRL incision were negligible in comparison to those produced using either Er:YAG laser or scalpel. Furthermore, protein signaling responsible for scar tissue formation was dramatically reduced with PIRL ablation, with no significant scar tissue formation extending away from the ablation margins. This significantly improved healing is presumable due to the very low thermal heating and energy transport to regions beyond the cut zone. To date, no study has directly measured and confirmed negligible tissue heating during active ablation using the PIRL system.

The objective of the current study is to measure and compare real-time heat generation during ablation of *ex vivo* porcine epidermis using a PIRL and conventional microsecond pulsed Er:YAG laser. It is hypothesized that real-time heat generation, as measured by infrared thermography, will be significantly lower for PIRL ablation than for Er:YAG laser ablation.

3.3 Materials and methods

3.3.1. Laser systems

An Er:YAG laser (MCL 29, Aesculap-Meditec GmbH, Heroldsberg, Germany) and a picosecond infrared laser (PIRL, AttoDyne Inc, Toronto, Canada) were used. The Er:YAG laser and PIRL had pulse lengths of 250 microseconds (250×10^{-6} seconds) and 300 picoseconds (300×10^{-12} seconds) respectively, both with wavelengths of 2.94 μm (microns). For the Er:YAG laser, a 5x1 mm slit mode was used. The Er:YAG system uses a scanning process, moving over the area under treatment in an overlapping fashion to ensure uniform ablation. The laser was set to produce 2 passes, at a pulse frequency of 24 Hz and pulse energy 100 mJ, corresponding to a fluence of 2 J/cm^2 for a 5x1mm slit. This fluence is only slightly higher than the ablation threshold of 1.5 J/cm^2 for soft tissue for Er:YAG laser, and lower than the typical fluence levels used in clinical applications such as skin resurfacing [87]. For the PIRL, a 5 mm line scan pattern was used. As with the Er:YAG laser, the PIRL system uses a similar scanning process moving over the area under treatment in an overlapping fashion, with the option of selecting the scan speed. The laser was again set to produce a total of 2 passes, with a scan speed of 3 mm/s and a pulse frequency of 50 Hz (the minimum setting for the PIRL system). The PIRL emits a circular Gaussian beam with a diameter of 300 μm. The pulse energy was measured at

0.2 mJ using a digital optical energy meter. The formula for peak Gaussian circular beam fluence (ϕ_0) is given by

$$\phi_0 = \frac{2 \cdot E_p}{\pi r^2}. \qquad \text{Eq 3.1}$$

Using Eq. 3.1, where E_p is the pulse energy and r is the beam radius, the corresponding output fluence of the PIRL was calculated to be 0.6 J/cm^2.

3.3.2. Thermography

Fresh *ex vivo* porcine full thickness skin sections (obtained from an abattoir within four hours of death and refrigerated at 4℃ until use) were cut into 1x1 inch sections from the dorsal hind leg region of a single specimen and centered within the laser focal plane. The capture field of a thermo camera (PIR uc 180, InfraTec, Dresden, Germany) was then focused onto this same region and calibrated. Thermography is based on the principle of blackbody radiation, whereby any opaque and non-reflective body will emit a characteristic electromagnetic radiation spectrum in a Gaussian curve dependent solely on its temperature. Thermography has been extensively used to study laser-induced temperature changes in various materials, including tissue [94-100]. The spectral range of the thermo camera used was 7.5 – 13 μm, selected in order to avoid capturing the thermal signal of the beam itself, at a much lower wavelength of 2.94 μm for both lasers. Real-time fast-frame thermal images (at 100 frames/second) were then captured for both systems during pulsed ablation. The peaks in the rises of skin temperature were determined using IRBIS 3plus software (InfraTec, Dresden, Germany). The IRBIS 3plus software generates 3 data points for each frame captured, at a rate of one frame every 10 ms. These 3 data points are the peak, minimum, and average temperatures, which can be independently calculated for user-defined regions within each thermal image frame. A

digital microscope was then used to capture post-ablation images to confirm the presence of superficial ablation craters within skin sections for both ablation methods.

Figure 3-1 shows the experimental thermography setup for the PIRL system. The output PIRL beam is shaped, focused, and combined with a low power helium-neon (red) beam for visibility and controlled with programmable beam-steering mirrors contained within an optics case (*a*). The skin sample is placed on the focal plane of the beam on a translation stage (*b*). The thermo camera is focused on the skin sample (*c*); its output is shown on the laptop screen (*d*). A digital microscope is focused on the sample (*e*); its output is shown on the desktop screen (*f*).

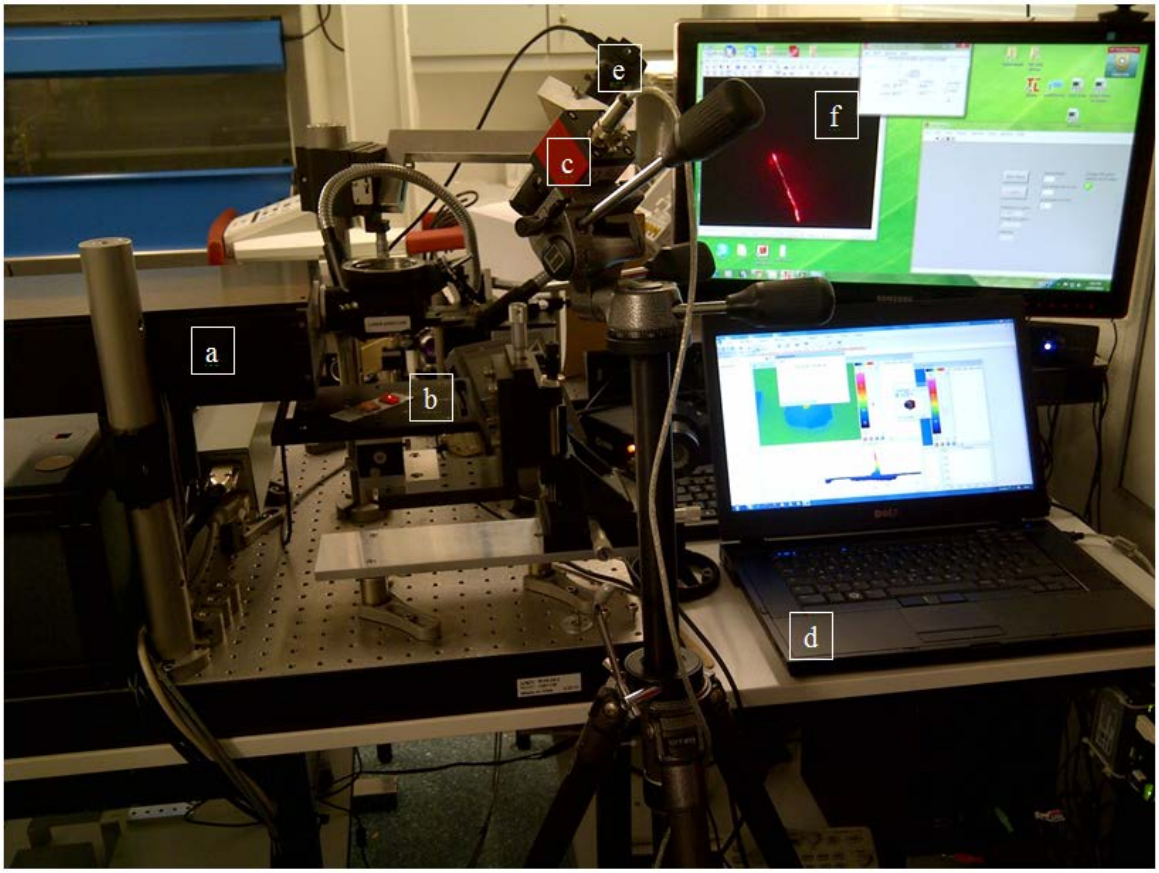

Figure 3-1: Experimental thermography setup for the PIRL system. (a) beam shaping optics, (b) skin sample on translation stage, (c) thermo camera, (d) thermo camera output screen, (e) digital microscope, (f) output screen of digital microscope.

3.3.3. Statistical analysis

Means of peak temperature recordings were comp aired using a a paired t-test with α set to 0.05. For a known standard deviation of 1 °C for the thermal images, a modest expected temperature rise of 10 °C for the Er:YAG laser ablation, and an α of 0.05, a single peak temperature measurement per laser would be required to detect a 25% difference in temperature rise between the two lasers with a power of 80%. In fact, twelve peak temperatures were measured and averaged for the Er:YAG laser in a 2-line pass, with hundreds of measurements recorded and averaged for the PIRL during ablation. Analysis was performed using SPSS 17.0 (IBM, Armonk, New York, USA).

3.4 Results

Figures 3-2 and 3-3 show representative thermal images captured during ablation for the Er:YAG laser and PIRL respectively. The images are colour mapped; the colour gradient on the right of each image demonstrates increases in temperatures from black/blue (cold) to violet/white (hot). Only thermal data within the white circular region (of approximately 7 mm diameter) is captured. As is clearly demonstrated, consistently significantly hotter regions are seen on the Er:YAG laser thermal images when compared to those generated using the PIRL. It is important to note that the colour gradient legend for the Er:YAG laser ablation varies from 29°C (black/blue) to 51°C (violet/white). The range of the colour gradient is narrower for the PIRL, from 28°C (black/blue) to 30°C (violet/white). The Er:YAG laser output beam (diameter of approximately 1 mm) is much larger than the PIRL (diameter 300 μm); as such, it is programmed to ablate in a larger stepwise overlapping fashion than is the PIRL. With the Er:YAG laser programmed to complete two-passes, a total of twelve pulses – and their resulting peak

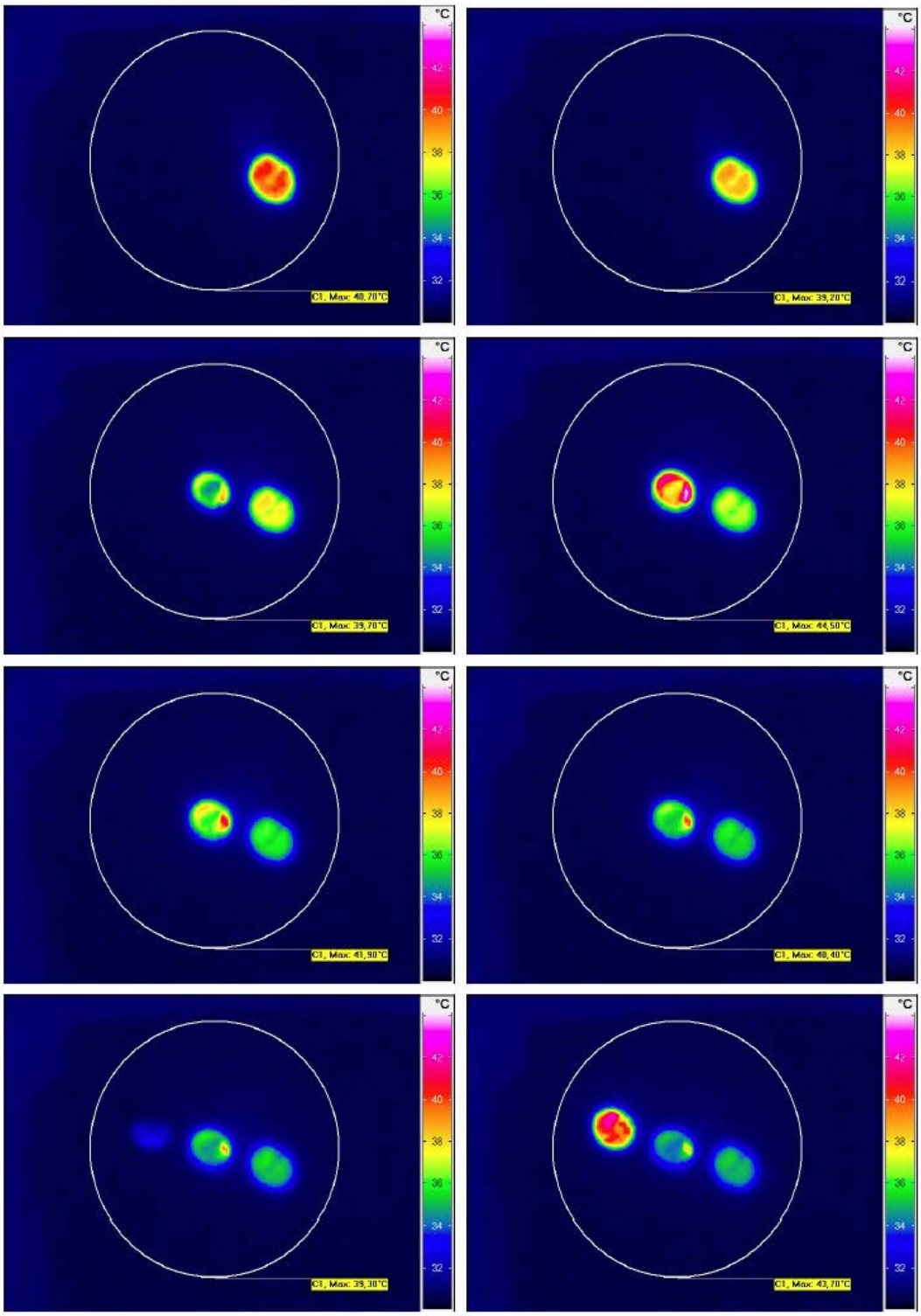

Figure 3-2: Representative thermal image frames from Er:YAG laser ablation.

temperatures – are delivered (three pulses are delivered going forward and three backwards, which is repeated in a 2-line pass). On thermal imaging, each delivered pulse

is seen as a distinct circular zone of approximately 1 mm in diameter (Figure 3-2). The PIRL is programmed to ablate with much smaller continuous steps, with a much higher pulse repetition rate, and thus shows a more linear pattern on thermal imaging (Figure 3-3).

The IRBIS 3plus software generates 3 data points for each frame captured, at a rate of one frame every 10 ms. These 3 data points are the peak, minimum, and average

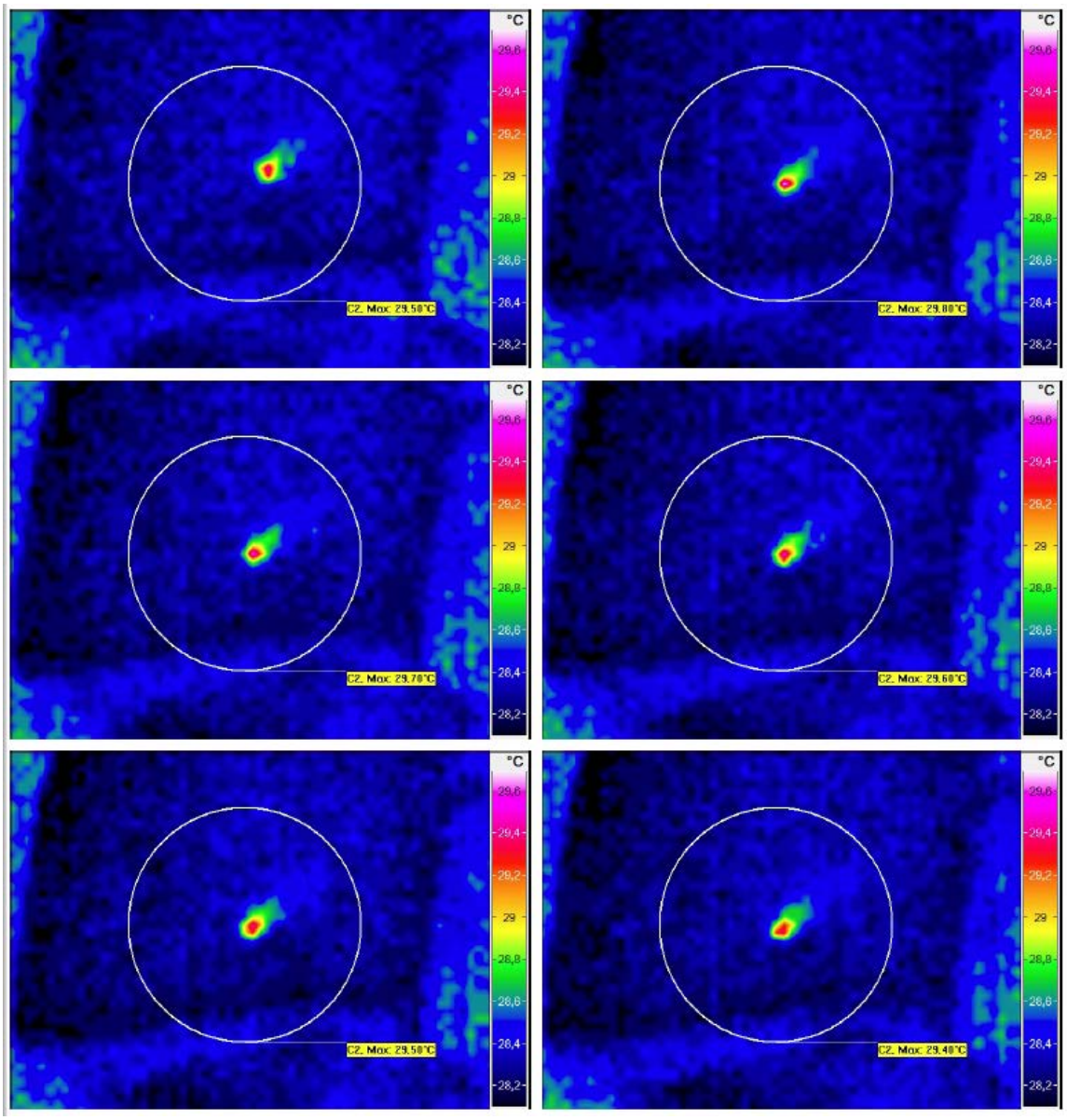

Figure 3-3: Representative thermal image frames from PIRL ablation.

temperature within the capture area contained by the white circle seen on the thermal images in Figures 3-2 and 3-3. These data points are then used to plot thermographs, line graphs of the peak, minimum, and average temperatures (y-axis) for 10 ms time intervals (x-axis). Figures 3-4 and 3-5 are thermographs of pulsed ablation for the Er:YAG laser and PIRL respectively. As would be expected for pulsed lasers, picket fence-like peaks are demonstrated. The highest line of peaks represents the maximum temperature, the middle line the average temperature within the entire capture field, and the lowest line the baseline skin surface temperature (essentially the room temperature for the *ex vivo* skin used). The baseline skin surface temperature was 30.2°C during Er:YAG laser ablation and 28.1°C during PIRL ablation. The warm baseline temperatures were the result overhead lighting combined with warm ambient room temperatures; experiments were conducted in two separate rooms as the laser systems could not be easily transported. As scanning patterns differ for Er:YAG laser and PIRL, different picket fence-like patterns are seen. In a two line pass, the Er:YAG laser thermogram shows two separate groupings of temperature peaks (Figure 3-4). The PIRL ablates in a continuous fashion (Figure 3-5). Despite the continuous pulsed nature of the PIRL ablation, heat generation during ablation remains significantly lower than during Er:YAG laser ablation.

The mean peak rise in skin surface temperature for the Er:YAG laser and PIRL was calculated at 15.0°C and 1.68°C, respectively ($p < 0.001$). Maximum peak rise in skin surface temperature was 18.85°C for the Er:YAG laser and 2.05°C for the PIRL. Ablation craters were confirmed on digital microscopy.

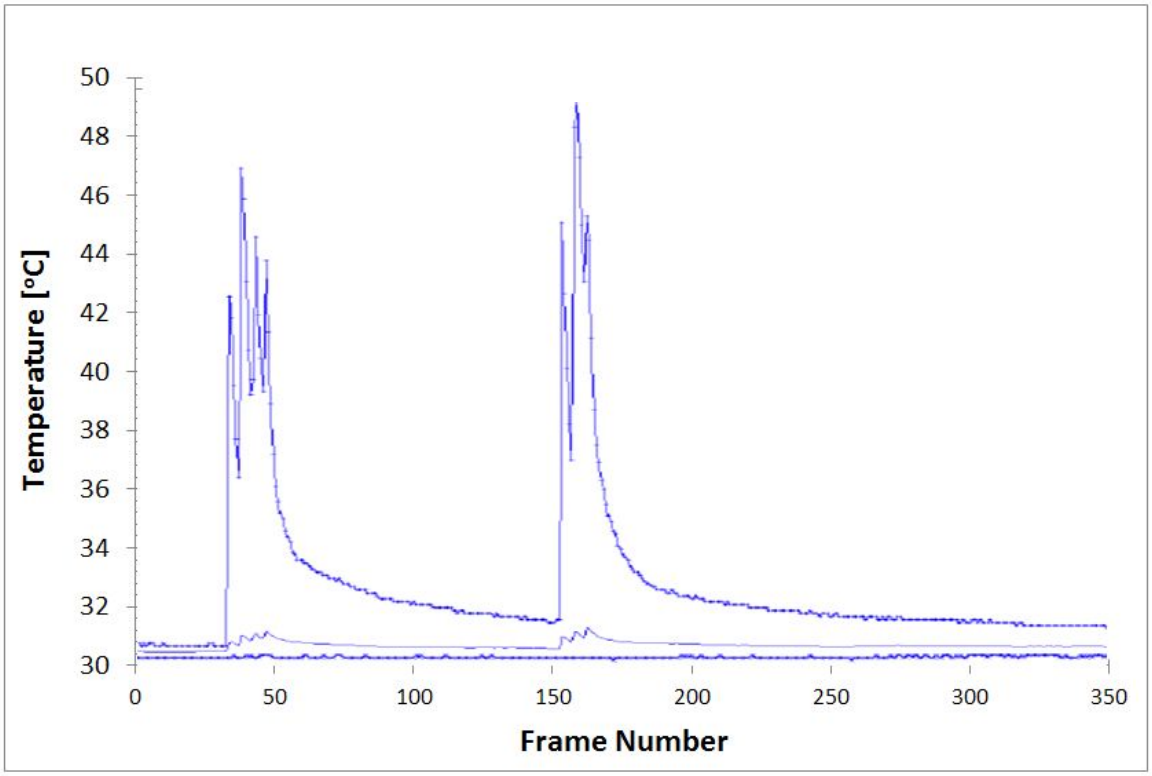

Figure 3-4: Thermogram for Er:YAG laser ablation (Temperature on y-axis vs. frame number on x-axis).

3.5 Discussion

Real-time heat generation during Er:YAG laser ablation of *ex vivo* porcine skin, as measured by thermography is significantly more than during PIRL ablation. At an Er:YAG laser ablation fluence of 2 J/cm^2, (just above the threshold fluence necessary for ablation to occur of 1.5 J/cm^2 for the Er:YAG laser), a mean temperature rise of 15°C and peak of 19°C was demonstrated. As discussed, irreversible thermal denaturation of human proteins may occur following short exposures to temperatures as low as 18°C above body temperature in the absence of thermal necrosis [45, 91-93]. Thus cellular injury may result despite this low Er:YAG laser fluence. Furthermore, such changes on a molecular level would not be immediately evident on standard histology. As such, measuring real-time heat generation during laser ablation is an important adjunctive

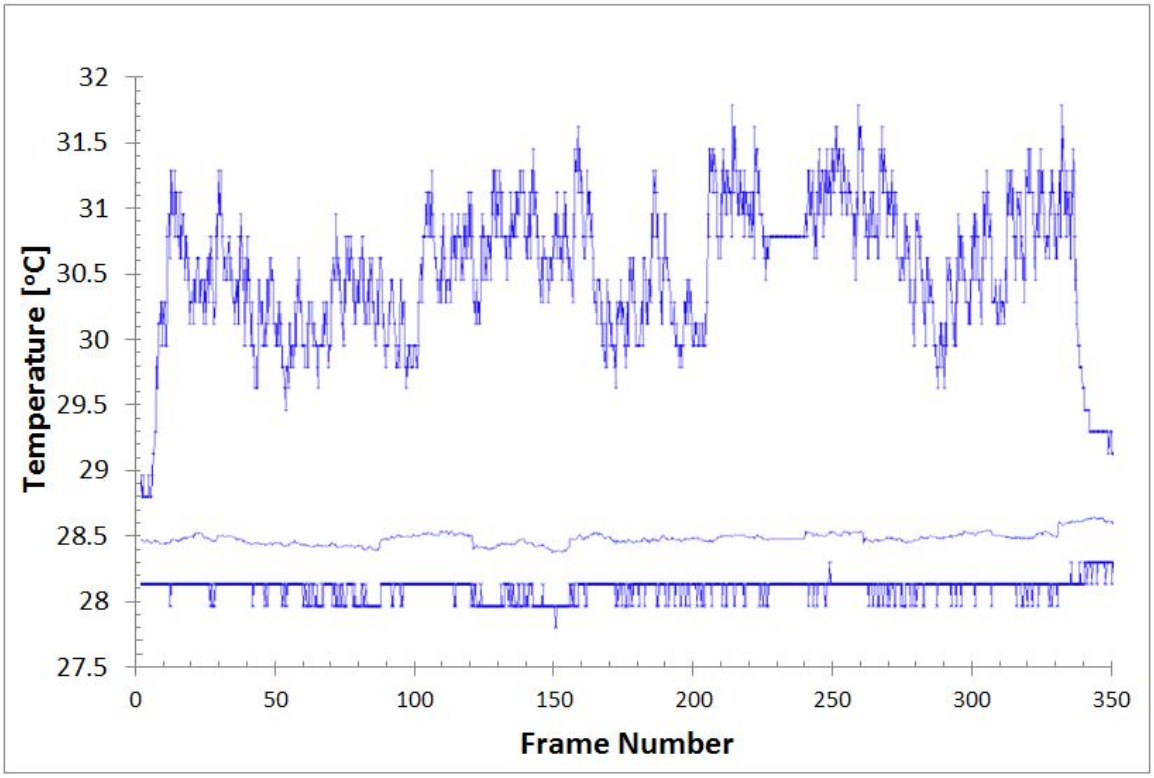

Figure 3-5: Thermogram for PIRL ablation (Temperature on y-axis vs. frame number on x-axis).

outcome measure. In clinical practice, much higher fluence levels are typically used, resulting in even higher peak temperatures [86-88, 102, 103].

The PIRL allows photon energy to be deposited in a much more efficient fashion, driving photomechanical ablation with near complete thermal confinement. As a result, the PIRL ablates at a much lower fluence than the Er:YAG laser. Only clinically negligible mean and peak temperature rises of 2°C were seen during active PIRL ablation using a fluence level sufficient for ablation by the PIRL of 0.6 J/cm^2.

3.5.1. Limitations of this study

This study is limited in that thermal characteristics of *ex vivo* skin differ from that of *in vivo* skin. Complex interplay of capillary blood flow and metabolic heat generation within in-situ skin is responsible for maintaining temperature homeostasis. In addition,

the water content and cellular integrity of *ex vivo* and *in vivo* skin differ considerably depending on time of harvest and preservation methods. In order to minimize these potential differences, skin samples used in this study were harvested fresh from an abattoir, refrigerated, and used within hours.

Additionally, the thermo camera used in this study had a frame capture rate limited to 100 Hz; frames are captured in 10 ms intervals. There will be some thermal diffusion during this time that will reduce the maximum temperature recorded in this sampling time. Despite this measurement limitation, there is a clear reduction in the excessive heat deposited adjacent to the ablated tissue zone with the PIRL system in comparison to the Er:YAG laser. Improvements in the time resolution of the thermal imaging would nevertheless be of significant value in correlating tissue damage and healing outcomes to the precise degree and duration of temperature elevations on adjacent tissue.

3.5.2. Future studies

It is interesting to note that use of the Er:YAG laser at a fluence just less than four times that used for the PIRL resulted in a nine-fold increase in peak temperature rise. This effect is in part due to the enhanced efficiency of the PIRL system in comparison to the Er:YAG laser; lower fluence rates – and hence less total energy deposition – are required to ablate a given volume of tissue. However, even after differences in fluence rates are accounted for, the adjusted thermal rise is more than double for Er:YAG laser ablation in comparison to PIRL ablation. The explanation for this difference is found by comparing the ablation dynamics of the two systems. In comparison with the Er:YAG laser, a significantly greater proportion of the PIRL's photon energy goes directly into

powering the photomechanical ablation process, with a much lower proportionate loss to energy spread outside the target area. The timescale is relevant; PIRL driven ablation occurs on a 100 ps timescale. With all short--pulsed lasers, some degree of excitation of recoil and acoustic modes within the target volume tissue occurs. In the nanosecond range and longer, these excitations propagate outwards from the target area causing additional heating and damage to the surrounding tissue as discussed above. In the picosecond range and shorter, the excited recoil and acoustic modes have frequency components on the order of 100 GHz (the Fourier transform of the ablation dynamics). Acoustics in this frequency range are strongly absorbed and hence do not propagate out of the ablation zone. The result is such that more energy is channeled into ablation instead of into heating of the surrounding tissue [8, 30]. The picosecond time scale also completely avoids other effects typically seen with conventional short-pulse lasers, such as nucleation growth and cavitation-induced shock waves, further increasing the ablation drive efficiency. The differences in temperature measurements between the two laser systems presented here are explained by these differences in their ablation dynamics.

Currently, the PIRL as currently set-up is limited to a fluence of 0.6 J/cm^2. Soon, more powerful PIRL systems will be available, with improved cutting speeds and tissue ablation rates. Similar experiments using these higher fluence levels will be required, as the dynamics of heat transport and acoustic propagation out of the ablation zone are non-linear; this characterization will be essential to ensure that PIRL scalpels are used at levels that retain negligible energy spread to adjacent tissue. Furthermore, standardization of ablation volumes will be necessary in future experiments to more precisely compare volume rates of ablation between laser systems.

In theory, photomechanical cold ablation should also be possible for osseous tissue using the PIRL, including cortical bone. Measurement of heat generation during PIRL ablation of osseous tissue is required as proof. In addition to *in vivo* soft tissue experiments to measure heat generation, more research is needed on longitudinal healing studies for both soft and osseous tissues.

3.6 Conclusion

This experiment has demonstrated that PIRL photomechanical ablation is a more efficient process than Er:YAG laser driven ablation. Furthermore, it has demonstrated that at fluence levels just above ablation threshold, temperature rises are negligible for PIRL ablation and significant for Er:YAG laser driven ablation.

The negligible heat generation as measured for PIRL ablation confirms the potential of this novel technology in minimizing undesirable thermal injury associated with lasers currently in clinical use. This study provides evidence for genuine cold ablation of soft tissue using a non-ionizing ultrafast picosecond pulse infrared laser system.

3.7 Acknowledgments

The authors would like to acknowledge Torsten König of InfraTec, GmbH (Dresden, Germany) for his assistance with the thermo camera operation and data assessment. They would like to acknowledge Dr. Wolfgang Kimmig, Department of Dermatology University Medical Centre Hamburg – Eppendorf for providing access to the Er:YAG laser.

3.8 Conflict of interest statement

R. Knecht is member of Advisory Boards of Merck Serono, Sanofi Aventis, Boehringer Ingelheim and Bayer Healthcare, Leverkusen. Prof RJD Miller and Dr Franjic are co-founders of AttoDyne Inc (manufacturer of the PIRL system). Prof Miller is author of a patent related to the mechanism of PIRL laser ablation.

3.9 Funding Sources

This research was sponsored, in part, by a resident research grant from the American Academy of Otolaryngology - Head and Neck Surgery Foundation (AAO-HNSF) Centralized Otolaryngology Research Efforts (CORE) grant program, a Canadian Institute of Photonic Innovations (CIPI) Technology Exploitation Network (TEN) grant, a Canadian Institute of Health Research (CIHR) Banting and Best M.Sc. Award, and a McGill Faculty of Medicine Graduate International Travel Fund.

4 Discussion and linking statements

4.1 Linking statement from first manuscript

As the study in the previous manuscript demonstrated, real-time heat generation during PIRL ablation of *ex vivo* porcine skin is negligible, far below levels required for protein alteration. In addition, the study demonstrated significant heat generation by Er:YAG laser ablation despite using very low fluence levels (only slightly above the ablation threshold for microsecond Er:YAG laser for skin).

4.2 Implications

The negligible heat generation as measured in real-time using thermography for PIRL ablation confirms the potential of this novel technology in minimizing undesirable thermal injury associated with current lasers in clinical use. Previous histologic studies have also shown that injury from transient acoustic effects is minimal with the PIRL [8, 11]. This study provides evidence for genuine cold ablation of soft tissue using an ultrafast infrared pulsed laser system at irradiance and fluence levels orders of magnitude below that which may cause free-radical production or ionization. Cold ablation is achieved through a photothermal mechanism using pulse widths meeting conditions for thermal and stress confinement, with material removal greatly enhanced through strong photomechanical effects.

4.3 Limitations of this study and linking statement to second manuscript

As discussed in the manuscript, this study is limited in that thermal characteristics of *ex vivo* skin differ from that of *in vivo* skin. Future studies must examine heat generation in the context of dynamic live skin in-situ. Ablation volumes need to be

standardized in order to compare ablation rates at similar fluence levels for the PIRL and Er:YAG laser systems. Importantly, the current PIRL system is limited to a maximum power output just below 1 J/cm^2. Once more powerful PIRLs are available, (which are currently under development), similar experiments at identical fluence levels will need to be carried out, to determine if temperature rises remain significantly lower for the PIRL at fluence levels similar to those used for Er:YAG laser. More powerful PIRLs would also permit for better characterization of material removal rates.

Standardizing the comparison of different laser systems in ablation is a challenging task. As in this study, the beam delivery systems (which may consist of any combination of glass or hollow core fibers, beam-steering mirrors, and focusing mirrors) often differ, producing different spot sizes and beam profiles. Secondly, ablation mechanisms differ and consequently the ablation threshold fluence differs between different laser systems. For example, in this study, a microsecond Er:YAG laser system was used without water spray. The principle ablation mechanism for such a system is photothermal vaporization via confined boiling and phase explosions, without meeting thermal or stress confinement conditions. As such, a significant amount of energy is lost from the target volume during ablation, and hence higher fluence levels are required to trigger material ejection (threshold fluence). The PIRL ablates principally via photothermal vaporization with phase explosions occurring at very low temperatures due to the significant thermoelastic photothermal effects as stress confinement conditions are met. As discussed in the introduction, these same photomechanical effects also trigger direct material fracture leading to material ejection. Since the PIRL mechanism involves containment of photon energy within the target volume, significantly lower fluence levels are required to trigger material ejection. Hence, it is more appropriate to compare

different laser systems at fluence levels relative to each system's specific ablation thresholds for a given tissue type. It is possible to use this approach while standardizing other variables, such as beam size, total energy deposited, and average power levels. The next chapter details a second experiment in manuscript form where attempts were made to standardize these parameters as much as possible, in comparing *ex vivo* bone ablation using Er:YAG laser versus PIRL.

5 Manuscript 2 – Ultrafast pulsed laser ablation of bone without thermal injury via a novel picosecond infrared laser (PIRL)

Nathan Jowett MD FRCSC[1,2*], Wolfgang Wöllmer PhD[2*], Paul Wiseman PhD[3], Alex M. Mlynarek MD MSc FRCSC[1], Balazs Lorincz MD[2], Kresimir Franjic PhD[4], Arne Böttcher MD[2], Rainold Knecht MD PhD[2], RJ Dwayne Miller PhD[4]

Submitted February 2013 for oral presentation at the American Academy of Otolaryngology – Head & Neck Surgery Annual Meeting, Vancouver, October 2013

Right of first refusal of manuscript reserved for *Otolaryngology – Head and Neck Surgery*

---

[1]Department of Otolaryngology – Head and Neck Surgery, McGill University, Montreal, Canada

[2]Department of Oto-, Rhino-, Laryngology, University Medical Centre Hamburg-Eppendorf, Hamburg, Germany

[3]Departments of Chemistry and Physics, McGill University, Quebec, Canada

[4]Atomically Resolved Dynamics Division, Max Planck Research Department for Structural Dynamics, University of Hamburg, Hamburg, Germany

*Author to whom correspondence should be addressed:

1. Dr. Nathan Jowett

Department of Otolaryngology – Head and Neck Surgery

Jewish General Hospital

3755 ch. de la Côte-Sainte-Catherine, Suite E-903

Montréal, QC, Canada H3T 1E2

Telephone: +1 514 340 8222 x8246, Fax: +1 514 340 7934

E-mail: nathan.jowett@mail.mcgill.ca

Article Type: Original Article

Section/Category: Reports of basic science

5.1 Abstract

Background and Objective: A precise method to ablate bone without significant thermal or acoustic injury has remained elusive. A novel non-ionizing ultrafast pulsed picosecond infrared laser (PIRL) may provide the solution. The PIRL ablates tissue through purely photomechanical means, via a thermo-elastic front spallation effect, with near complete thermal and acoustic transient confinement. In contrast, the Er:YAG laser ablates tissue via a micro-explosive vaporization mechanism. This study compares PIRL and Er:YAG laser ablation of bone by infrared thermography (IRT), digital and electron microscopy.

Methods: Ten cuts were made in fresh *ex vivo* cortical bone via PIRL and Er:YAG laser ablation under IRT imaging using similar average power settings. Digital microscopy was used to image the ablation zones.

Results: Peak temperature spikes were negligible and significantly lower for PIRL in comparison to Er:YAG laser ablation (1.56 ± 2.7°C vs. 12.99 ± 2.7°C, $p = 0.008$). Digital microscopy confirmed cortical surface ablation for both lasers, with no sign of micro-fracture for either ablation method.

Conclusion: The PIRL provides a means of cortical bone ablation without shockwave induced micro-fractures. This novel laser has great potential in advancing surgical techniques and outcomes in otologic, neurotologic, implant, cranio-maxillofacial, and head and neck reconstructive surgery.

Keywords: laser ablation, cold ablation, picosecond infrared laser, Er:YAG laser

5.2 Introduction

Cutting densely calcified tissue in surgery typically necessitates the use of crude instruments such as saws and drills. These instruments are known to generate significant tissue damaging heat and vibrations [1, 2]. Osseous temperatures higher than 100°C have been recorded during bone removal with mechanical burrs despite the use of a liquid coolant [18]. Heating osseous tissue above 60°C has consistently been shown to inactivate alkaline phosphatase, interrupt blood flow, and cause tissue necrosis leading to delayed tissue healing [1, 19-21]. Heating to a temperature as low as 50°C for one minute may lead to bone resorption and replacement of bone with fat cells [20]. In osseous surgery, such as mandible reconstruction, delayed healing has the potential to lead to disastrous consequences in the form of fibrous non-union [3]. In osseous drilling for implantation of osseointegrated devices such as dental implants or bone anchored hearing aids (BAHA), thermal damage can lead to failure of osseointegration[22]. Furthermore, mechanical instruments carry significant risk of plunging injuries and collateral damage to adjacent vital soft tissue structures [4]. In regions of dense critical anatomy such as the head and neck, the risk of collateral damage is of particular concern.

The invention of the laser in 1960 by Maiman was met quickly with unbridled optimism for improving surgical precision and healing outcomes across a myriad of disciplines. Indeed, lasers have since proven invaluable in soft-tissue applications in ophthalmology, dermatology, and otolaryngology [23]. More recently, the pulsed erbium-doped yttrium aluminium garnet (Er:YAG) laser showed promise for efficient ablation of densely calcified tissue [104, 105]. The combination of a short pulse length (on the scale of microseconds to nanoseconds), and a wavelength of 2.94 μm (corresponding to the absorption coefficient peak of water in the mid-infrared region)

allows for efficient photo-thermal explosive vaporization leading to material ejection. However, despite the short pulse lengths, complete thermal confinement is not possible due to non-uniform longitudinal and transverse absorption profiles [8]. Furthermore, the propagation of photo-acoustic energy out of the ablation zone, which occurs on a time scale on the order of 1 ns, leads to further tissue injury [8, 30]. Healing studies on bone following Er:YAG laser ablation have consistently demonstrated a mineral-rich amorphous peripheral damage zone. Despite spanning only a few microns, this layer results in markedly delayed healing due to its resistance to absorption when compared to conventional surgical osteotomy by saw or burr [71, 106, 107].

The development of a picosecond infrared laser (PIRL) at 2.94 μm seeks to circumvent the undesirable spread of photon energy away from the target volume. By taking advantage of the ultrafast energy transfer between the vibrationally excited intramolecular O-H bond stretching modes and the intermolecular oscillations of the hydrogen bond network of water molecules (which occurs with complete thermalization within several picoseconds), the PIRL is capable of explosive photo-thermal vaporization with near complete thermal confinement [8, 30]. Importantly, the picosecond timeframe also results in near complete stress confinement, while avoiding ionization and multiphoton effects than occur with femtosecond pulses. As a result of negligible energy loss outside of the ablation volume, ablation efficiency is markedly improved. Initial studies with the PIRL demonstrated an ablation threshold of only 0.5 – 0.75 J/cm^2 for enamel [8]. In comparison, the threshold ablation of enamel using Er:YAG laser is around 10 J/cm^2 [108]. Initial soft tissue healing studies have shown significant benefit of PIRL ablation incisions over Er:YAG laser and conventional surgical scalpel incisions [11]. *Ex vivo* vocal fold and laryngeal cartilage incisions made with PIRL have

demonstrated near complete absence of thermal injury and much narrower cutting haps when compared to CO_2 laser [109]. Thermography has shown significantly lower *ex vivo* skin surface temperature rise during ablation using PIRL when compared to Er:YAG laser [110]. The objective of this study is to objectively compare surface temperature rise by means of thermography during ablation of *ex vivo* bone by means of PIRL and Er:YAG laser.

5.3 Materials and methods

5.3.1. Laser systems

A picosecond infrared laser (PIRL, AttoDyne Inc, Toronto, Canada), and an Er:YAG laser (MEY-1-A EX-2, J. Morita Mfg. Corp., Kyoto, Japan) were used. The PIRL and Er:YAG laser had pulse widths of 300 ps and 300 µs respectively, both having wavelengths of 2.94 µm with approximately Gaussian cross-sectional profiles. The PIRL system had an adjustable repetition rate between 50 Hz and 250 Hz, and adjustable pulse energy from 0% to 100%. The Er:YAG laser system had an adjustable repetition rate between 1 Hz and 25 Hz, and adjustable pulse energy from 10 mJ to 400 mJ. The PIRL system beam was coupled to x-y galvo mirrors programmed for 800 µm diameter (*d*) circular area scanning at the focal point, visualized with a low-energy helium-neon (HeNe) laser beam along the same path as the 2.94 µm PIRL output beam. The Er:YAG laser system beam, housed within a flexible hollow-fiber articulating arm with distal hand-piece, was coupled to a 800 µm diameter glass fiber tip (C800F, J. Morita Mfg. Corp., Kyoto, Japan)(Figure 5-1). For comparative purposes, average power, average irradiance/intensity (average power per unit area), and total deposited energy were matched as closely as possible between the two systems. For the PIRL, a repetition rate

Figure 5-1: Glass fiber Er:YAG laser handpiece tip (800 µm).

of 250 Hz with pulse energy (E_p) set to 100% output resulted in a measured average power of 69.1 mW, corresponding to an average irradiance of 13.7 W/cm^2 over a 800 µm diameter circular scanning area. For the Er:YAG laser, a repetition rate of 3.3 Hz with a pulse energy set to 30 W resulted in a measured average power of 67.6 mW, corresponding to an average irradiance of 13.4 W/cm^2 at the tip of the 800 µm diameter circular glass fiber. Power measurements were done for both systems using a precision power and energy meter (LabMax-TOP with PowerMax PM3 detector, Coherent Inc., Santa Clara, CA, USA). (Measured average power was below specified as a result of typical fiber-coupling losses for the Er:YAG system). Using the average power measurements, total ablation time necessary to deposit 1 J of total energy onto the 800 µm diameter circular tissue area was calculated to be 14.5 s and 14.8 s for the PIRL and

Er:YAG laser respectively. Pulse fluences for both systems were above their respective threshold levels for ablation of bone, while far below levels required for plasma formation. Peak fluence levels were calculated using the formula for Gaussian beam fluence (ϕ_p), given by

$$\phi_p = \frac{2 \cdot E_p}{\pi(\frac{d}{2})^2}. \qquad \text{Eq 5.1}$$

Peak pulse fluence levels and a summary of laser parameters are summarized in Table 5.1.

Table 5.1: Laser system parameters.

Parameter	PIRL	Er:YAG Laser
Wavelength (λ)	*2.94 µm*	*2.94 µm*
Beam diameter (*d*), profile	*300 µm, Gaussian*	*800 µm, Gaussian (approx.)*
Pulse width	*300 ps*	*300 µs*
Area of ablation	*0.0050 cm^2*	*0.0050 cm^2*
Scanning pattern	*Circle (d = 800 µm)*	-
Repetition rate	*250 Hz*	*3.3 Hz*
Average power	*69.1 mW*	*67.6 mW*
Pulse energy *(E_p)*	*0.276 mJ*	*20.484 mJ*
Peak pulse fluence (ϕ_p)	*0.78 J/cm^2*	*8.15 J/cm^2*
Peak power	*9.21 x 10^5 W*	*68 W*
Peak irradiance (peak power density)	*1.3 GW/cm^2*	*0.13 MW/cm^2*
Ablation time	*14.5 s*	*14.8 s*
Total energy deposited	*1 J*	*1 J*

5.3.2. Thermography

Thermography is based on the principle of blackbody radiation, whereby any opaque and non-reflective body will emit a characteristic electromagnetic radiation spectrum in a Gaussian distribution dependent solely on its temperature. Thermography has been extensively used to study laser-induced temperature changes in various materials, including tissue [94-100]. A thermo camera (PIR uc 180, InfraTec, Dresden,

Germany) having a spectral range of 7.5 – 13 µm was used in order to avoid capturing the thermal signal of the beam itself, at a much shorter wavelength of 2.94 µm for both lasers.

5.3.3. Ablation procedure

A fresh, refrigerated *ex vivo* chicken femur harvested within 48 hours of animal sacrifice was passively warmed to room temperature. The same specimen was used for both PIRL and Er:YAG laser ablation trials, which were conducted in immediate sequence on the same specimen stage in the same laboratory. This method was selected to minimize any potential differences in temperature and/or humidity within the laboratory, as well as any potential differences in temperature, humidity, and tissue integrity within the specimen during ablation trials comparing the two laser systems. The femur was initially positioned onto the adjustable z-axis (vertical) micrometer specimen stage and brought into the focus point of the PIRL beam. The capture field of the thermo camera was then focused onto this same region and calibrated. Ten ablation trials consisting of the deposition of 1 J of total energy each were run for each laser system. The Er:YAG laser used in this study was specifically manufactured with a hand-piece that integrates tunable sterile water and air flow at the beam output, whose purpose serves for the removal of ablation debris (and blood during *in vivo* use) from the surface of the ablation field and from the end of the glass fiber delivery tip to prevent loss of energy delivery. The water flow also helps drive the photomechanical ablation process, which is dependent on a hydrated ablation field. Additionally, it serves to reduce undesirable heating. The water and air flow settings on the Er:YAG laser hand-piece tip are independently adjustable between settings of 0 and 10, and may be used with or without the Er:YAG laser beam activated. As the PIRL did not have an integrated water/air flow

system, to standardize the comparisons as much as possible the same Er:YAG laser hand-piece integrated water/air flow system was used for all trials with a setting of ‘10’ for air (approximately 2.5 mL/min) and ‘1’ for water flow (approximately 2.0 mL/min). For both PIRL and Er:YAG laser ablation trials, the Er:YAG laser glass-fiber tip was positioned stationary in close contact with the tissue surface at a 45° angle away from the normal angle (in the same fashion that it is designed to be used clinically). The integrated low-energy visible HeNe laser steering beam on the PIRL permitted for precise placement of the Er:YAG hand-piece glass-tip immediately adjacent to the ablation field, ensuring the water and airflow dynamics for both types of laser ablation were identical. The Er:YAG laser also incorporates a visible HeNe steering beam, which was switched on during Er:YAG laser ablation and power measurements as it was during PIRL ablation and power measurements to standardize the comparisons. Furthermore, the integrated HeNe beams on both systems were of such low-energy that any potential effect on either total power or temperature measurements was negligible.

Figure 5-2 demonstrates the experimental thermography setup for PIRL ablation. The output PIRL beam was shaped, focused, and combined with a low power helium-neon (red) beam for visibility and controlled with programmable beam-steering x-z galvo mirrors contained within an optics case (*a*). The femur was placed on the specimen stage and brought into the focal plane of the beam (*b*). The thermo camera wass focused onto the same focal plane (*c*) with output shown on the laptop screen (*d*). A digital microscope was similarly focused on the sample focal plane (*e*) with output shown on the desktop screen (*f*). A beam energy meter is also shown (g). In all trials, the Er:YAG hand-piece was postioned immediately adjacent to the PIRL focal area in the fashion described above

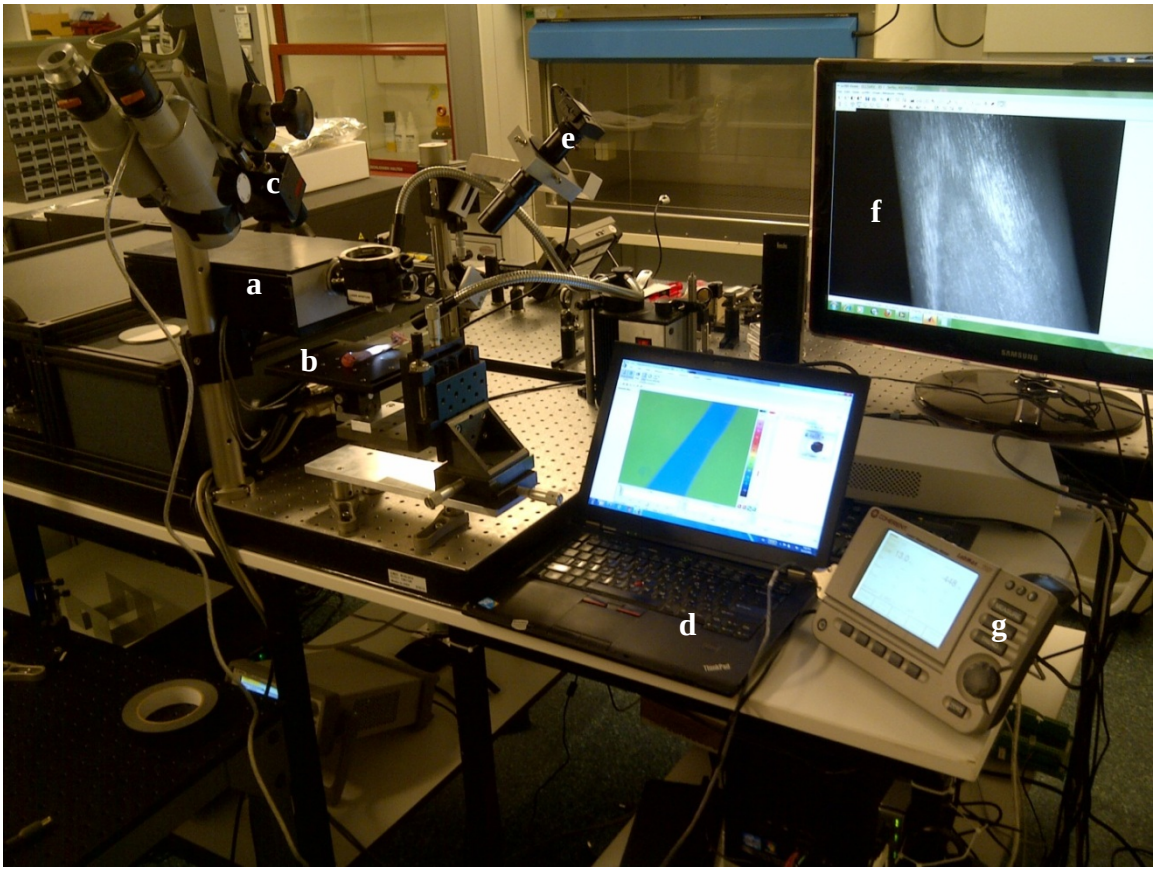

Figure 5-2: Experimental setup. Beam-steering x-z galvo mirrors contained within an optics case (*a*), specimen stage (*b*), thermo camera (*c*), output of thermo camera (*d*), digital microscope (*e*), digital microscope output (*f*), and energy meter (g).

(not shown), such that air and water flow during thermography recodings was identical for both ablation methods.

5.3.4. Image capture

Real-time fast-frame thermal images (at 100 frames/second) were captured for both systems during the pulsed ablation trials. IRBIS 3Plus software (InfraTec, Dresden, Germany) was used to capture and analyze the thermal images. For an ablation time of 14.5 s for the PIRL, a total of 1450 thermal image frames were analyzed for each of the ten PIRL trials (each frame representing integrated 10 ms time intervals). Similarly, for an ablation time of 14.8 s for the Er:YAG laser, a total of 1480 frames were analyzed for

each trial. From initial trials, it was noted that the tissue surface temperatures quickly reached a steady-state within 2 s of laser activation for both systems. Thus thermal measurements were started 2 s after laser activation in all trials. Digital microscopy was then used to capture post-ablation images to confirm and qualitatively compare the presence of superficial ablation craters within the outer cortical layer of the chicken femur for both ablation methods.

5.3.5. Statistical analysis

The average rise in surface temperatures across all trials between the two laser systems was plotted and the means determined (listed ± SD with 95% confidence intervals) and compared using a two-sided t-test. Additionally, peak rises in surface temperature corresponding to pulsed spikes in temperature between the two systems were compared without averaging by using a mixed measures ANOVA test with means listed ± SEM (standard error of the mean) with 95% CI (confidence intervals). For all comparisons, α was set at 0.05. Scatterplots were made using Microsoft Excel 2010 (Microsoft Corp., Redmond, WA, USA). IBM SPSS Statistics 20 (IBM Corp., Armonk, New York, USA) was used for statistical tests.

5.4 Results

5.4.1. Thermal imagery

Thermal images series were captured for all ablation trials and analysed. Figures 5-3 and 5-4 demonstrate frame captures from PIRL and Er:YAG laser ablation trials. The IRBIS 3Plus software calculates minimum, maximum, and mean temperature within user-defined geometric areas for each thermal image frame series. Three separated circular regions were defined within each thermal image series. The first region (approximately 3

mm in diameter) was centered on the ablation zone in order to calculate the ablation zone maximum surface temperature (AMaST). Another region (approximately 1 mm in diameter) was centered of the path of water and airflow as it exited the fiber tip, outside of the ablation zone, to determine the water and airflow mean temperature (WMeT). The third region selected (2 mm in diameter) in order to determine the baseline mean surface temperature (BMeST) of the femur within the same plane of focus, while outside of the path of water and airflow and away from the ablation zone. These regions may be seen in Figures 5-3 and 5-4. Thermograms were then plotted using IRBIS 3Plus for each trial plotting AMaST, WMeT, and BMeST against time. Representative thermograms are

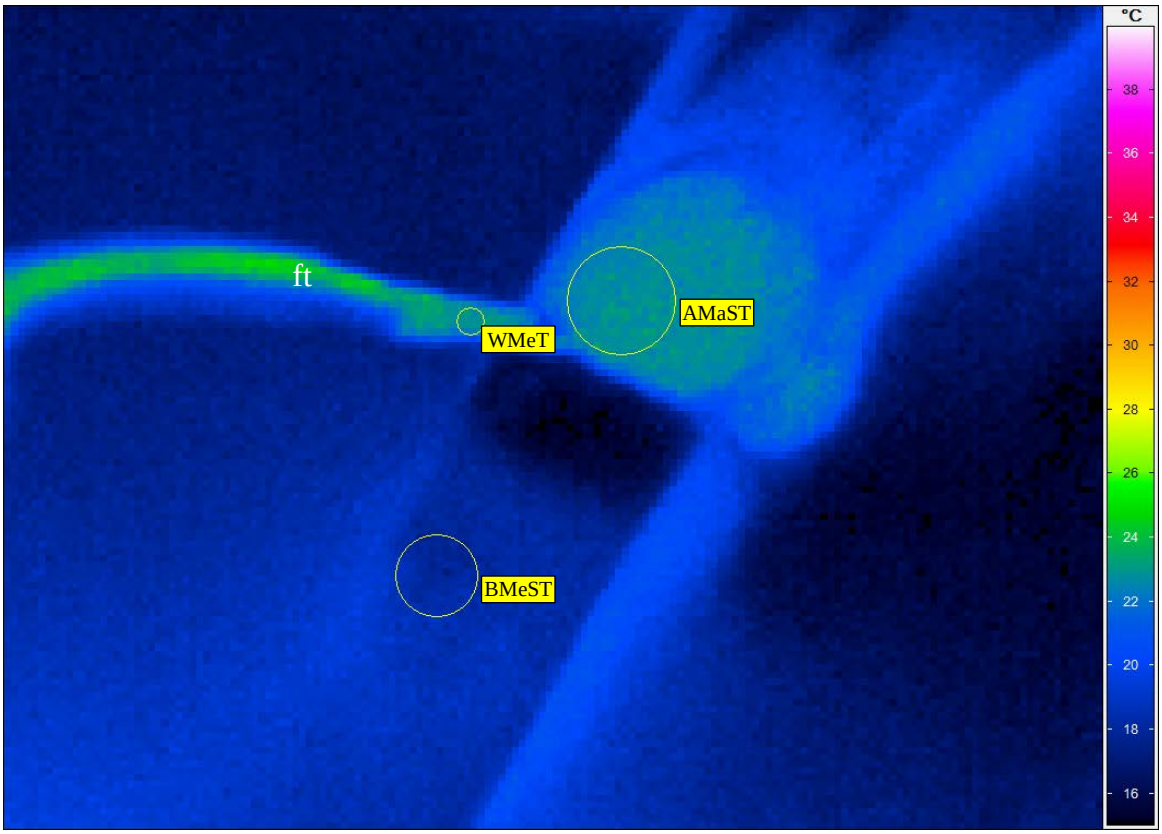

Figure 5-3: Sample PIRL ablation thermal image. Fiber tip with air and water spray is seen at left (ft). Temperature gradient legend is inset at right. Three circular zones are demonstrated within which temperatures were recorded as follows: ablation zone – maximum surface temperature (AMaST), water and airflow – mean temperature (WMeT), bone surface far from ablation zone – mean surface temperature (BMeST).

shown in Figures 5-5 and 5-6. As the area of ablation was constantly under water and airflow irrigati on, rises in temperature due to laser ablation were calculated by subtracting the WMeT from the AMaST to obtain an absolute temperature rise in degrees Celcius. (The BMeST is shown for reference purposes only and was not used in calculations; considering the high thermal conductivity of water, the baseline surface temperature of the region of bone under constant irrigation was assumed to be approximately equal to the WMeT for all trials). Considering the low pulse energy and high repetition rate of the PIRL, it is not surprising that minimal fluctuations in the AMaSTs are seen during PIRL ablation (Figure 5-5). With Er:YAG laser ablation, however, higher pulse energies and a lower repetition rate generate repetitive rapid bursts in the AMaSTs (Figure 5-6).

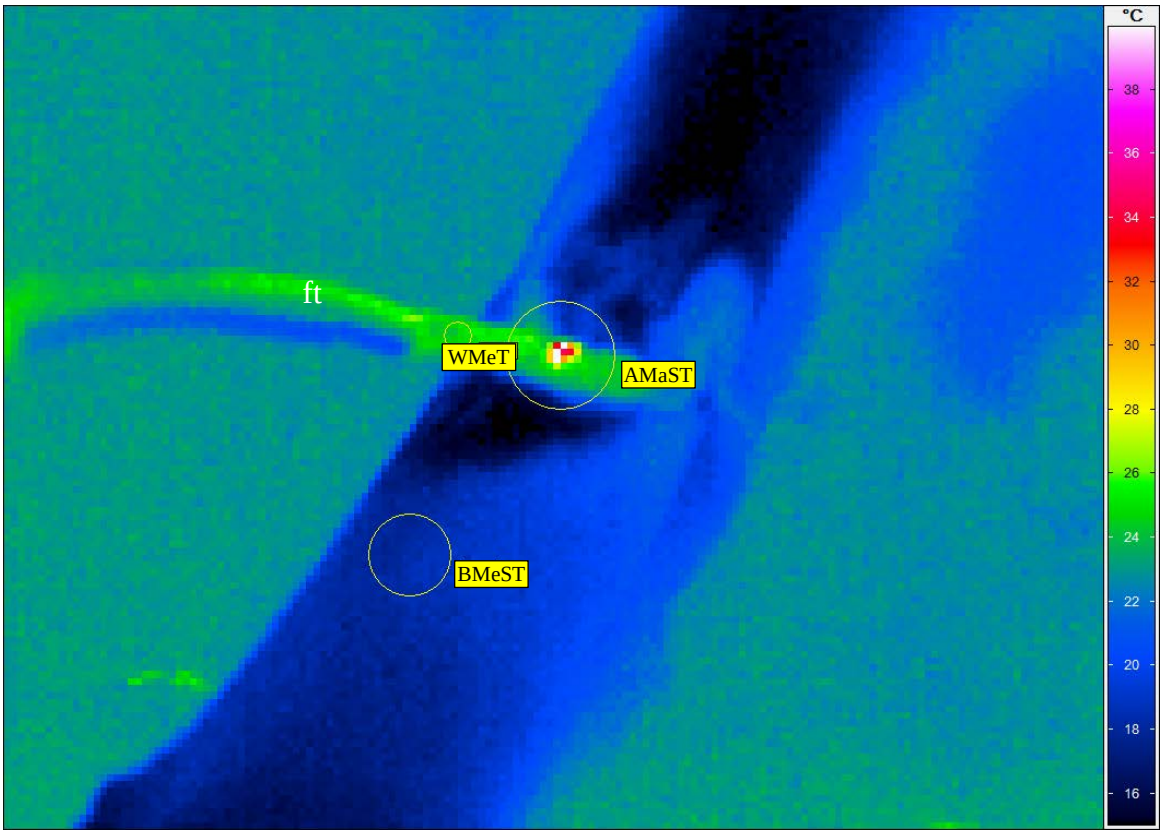

Figure 5-4: Sample Er:YAG laser ablation thermal image. See caption for Figure 5-3.

5.4.2. Digital microscopy

Digital monocular microscopy confirmed the presence of superficial ablation craters within the outer cortical layer of bone for both ablation methods (Figure 5-7 and 5-8). No carbonization is seen in either specimen.

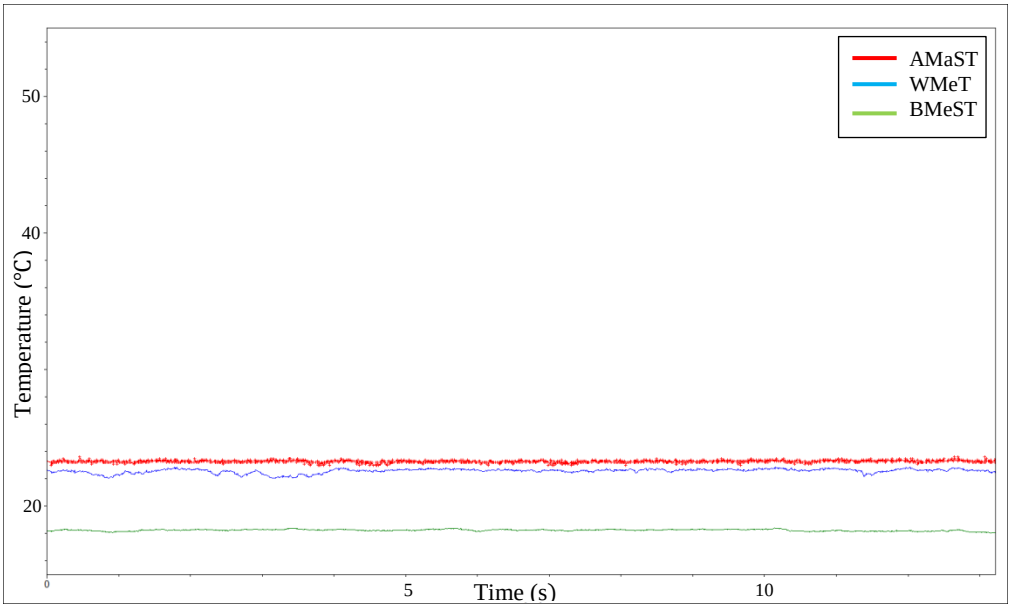

Figure 5-5: PIRL ablation thermogram. AMaST = ablation zone maximum surface temperature, WMeT = water and airflow mean temperature, BMeST = baseline femur mean surface temperature.

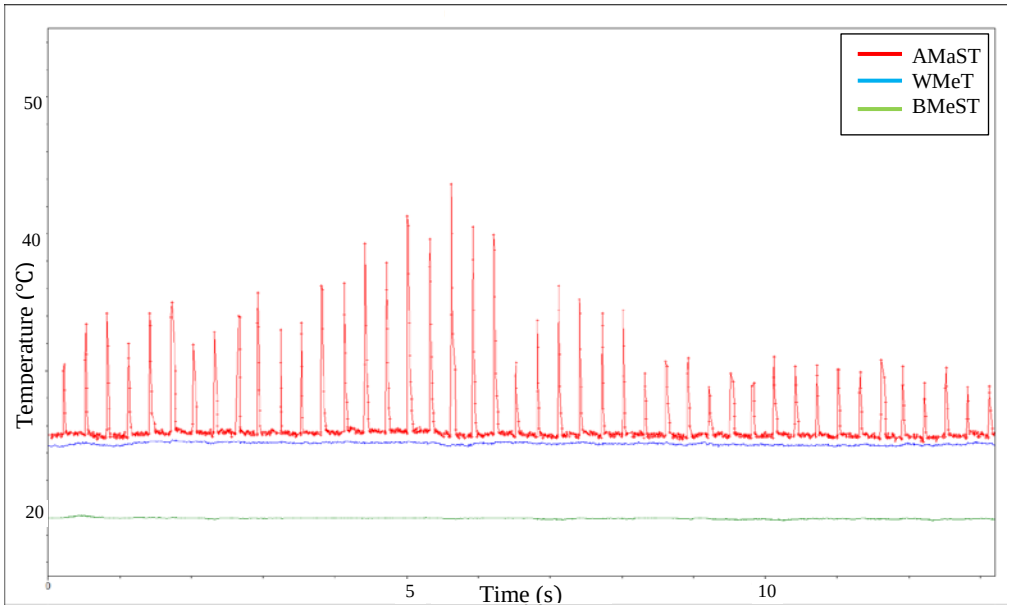

Figure 5-6: Er:YAG laser ablation thermogram. See caption for Figure 5-5.

5.4.3. Statistical analysis

Increases in surface temperature within the ablation zones were calculated across all frames for all trials for PIRL and Er:YAG laser. Data was then analyzed in two separate clusters. The first cluster consisted of all data points, averaged over all ten trials for PIRL and Er:YAG laser ablation respectively. The mean rise in surface temperature across the entire ablation period was minimal for both systems, yet statistically lower for

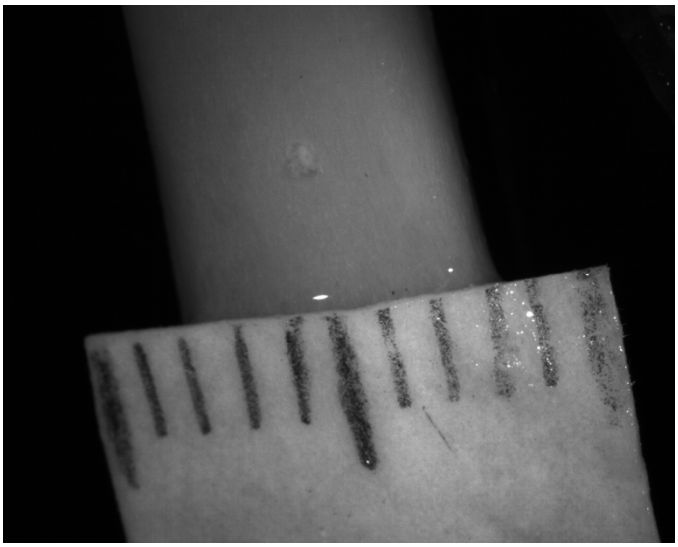

Figure 5-7: PIRL ablation crater. Millimeter scale shown.

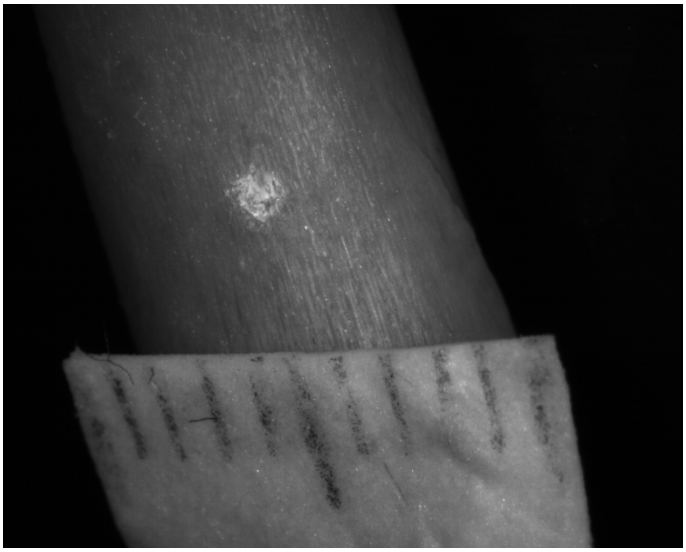

Figure 5-8: Er:YAG laser ablation crater. Millimeter scale shown.

PIRL ablation at 0.78 ± 0.73°C (95% CI: 0.77°C to 0.79°C) compared to Er:YAG laser ablation at 1.70 ± 3.53°C (95% CI: 1.64°C to 1.75°C) ($p < 0.001$).

Comparison of mean tissue temperature alone when analyzing pulsed laser systems by means of continuous frame capture thermography can be misleading due to thermal diffusion out of the excited zone (heat loss) relative to the laser repetition rate. As is clear from the Er:YAG laser ablation thermogram in Figure 5-6, rapid rises and falls in temperature occur, while the majority of data points remain far below the peak temperature rises. In order to better account for these temperature spikes, a subset of data consisting of the highest temperature recordings for each trial was analysed (corresponding the peaks seen in Figure 5-6). Analysis of these temperature spikes showed an average rise of 1.56 ± 2.71°C (95% CI: -4.14°C to 7.27°C) for PIRL ablation and 12.99 ± 2.71°C (95% CI: 7.29°C to 18.70°C) for Er:YAG laser ablation ($p = 0.008$).

5.5 Discussion

Mechanisms of laser ablation of tissue include photothermal, photomechanical, photochemical (also known as ablative photodecomposition), and plasma-mediated [5, 28]. Of these, the latter three involve photon energies or densities causing ionization and hence are not suitable for use on regenerating tissue. This study has compared two laser systems that target the absorption coefficient peak of water around 3 μm that ablate by means of photothermal vaporization. In order to standardize the comparison, average powers were matched as closely as possible while using appropriate fluence levels for each system. For the Er:YAG laser, the threshold for bone ablation has previously been found to be on the order of 2-3 J/cm^2 (three to fivefold less than the respective threshold for enamel).[86] The peak fluence of 8.15 J/cm^2 for Er:YAG laser ablation used in this

study is well within the therapeutic window of 3.4-16 J/cm^2 described by Walsh et al., below which energy is absorbed into the tissue primarily as heat without ablation and above which thermionic plasma formation may occur [86]. The supra-threshold peak fluence chosen also serves to minimize the amount of sub-ablation level energy present at the fringes of the roughly Gaussian cross-sectional beam. Furthermore, the supra-threshold level chosen also permits for continued ablation in the face of precipitous fluence losses of up to 50% with inadvertent tip-tissue separation distances as small as 1 mm [104]. The threshold fluence for PIRL ablation of bone has not yet been precisely determined, although it can be reasonably assumed that it is less than its respective ablation threshold for enamel (known to be between 0.5 J/cm^2 and 0.75 J/cm^2) [8]. The peak fluence of 0.78 J/cm^2 for PIRL ablation used in this study is well below levels required for plasma formation, and thus falls within a respective supra-threshold treatment window adequate for objective comparison with Er:YAG laser ablation.

In this study, it is the peak temperature rise that is the most relevant parameter. As can be seen in Figure 6, the thermal diffusion time is barely resolved within the detector response time and it is on the order of 30 ms. This measurement is consistent with estimates for thermal diffusion based on the thermal diffusivity of water. Taking this into account, there are approximately 10 decades in time for the temperature to decay back to near ambient between lase shots for the Er:YAG ablation study. However, the peak temperature is most telling. Given the finite detector response, the measured values must be taken as lower limits. Taking thermal diffusion effects into consideration, the results of this study clearly demonstrate, peak surface temperature rises during ablation remain significantly lower for the PIRL than for the Er:YAG laser at 2°C compared to 13°C, respectively. Again, this peak temperature is a lower limit due to the finite detector

response time relative to thermal diffusion out of the excited zone that lowers the measured temperature. The important point is that the peak temperature rise is a factor of 5 times smaller than with Er:YAG laser ablation. This difference is quite significant and is a direct consequence of the much more efficient mechanism for laser ablation with the PIRL system relative to the conventional Er:YAG laser. The small temperature rise that occurs with PIRL ablation may be considered clinically negligible, as temperatures rises greater than 10°C (assuming a body temperature of 37°C) are typically required to cause bone injury [20]. Furthermore, the time scale for the temperature rise to cause damage depends on the overall integrated time the system is exposed to an elevated temperature. The whole process occurs on picosecond timescales with PIRL and as such this relatively small peak excursion in temperature can be considered negligible, as evidenced by the complete conservation of tissue characteristics of the adjacent tissue with no noticeable damage both in this study and previous work [8, 109, 110]. The reason for the significant dampened temperature rises seen with PIRL and lack of collateral tissue damage in comparison to Er:YAG laser ablation stems from the shorter and more efficient method of energy deposition that is possible on the picosecond scale. In depositing photon energy on a time scale several orders of magnitude shorter than both typical tissue thermal relaxation times (measured in microseconds) and stress confinement times (measured in nanoseconds), the picosecond infrared laser ablates tissue with negligible energy spread outside of the target volume. In addition to lower temperatures, PIRL ablation occurs without the characteristic popping sound common to Er:YAG laser ablation which limits its application in critically noise-sensitive otologic surgery such as stapedotomy [73]. Further studies will seek to precisely quantify any potential acoustic effects of PIRL ablation, as this technology may become an important tool in otologic surgery.

5.5.1. Study limitations and future directions

This study is limited in that temperature measurements were conducted with use of active air and water irrigation. Water irrigation serves to hydrate the tissue (which helps to drive the ablation process) as well as to provide cooling. With *ex vivo* compact bone – such as the type used in this study – dehydration occurs rapidly without water irrigation, leading to a swift decrease in ablation efficiency. Following dehydration, incident photons are primarily absorbed by hydroxyapatite molecules, which like water molecules also demonstrate an absorption coefficient peak around 3 μm [111]. Unlike water molecules however, they do not undergo the same rapid thermalization; instead of material ejection , photon absorption by hydroxyapatite at low fluence levels leads to significant lattice heating. This occurs for both PIRL and Er:YAG laser. Dehydration becomes less of an issue in live compact bone, which remains significantly more hyrdrated than *ex vivo* bone due to its Haversian system. Future studies will quantify tissue heating during PIRL ablation on *in vivo* bone without irrigation, in addition to examining healing outcomes. In theory, the negligible thermal and acoustic cellular insults possible with PIRL ablation of bone may potentially lead to improved healing outcomes in comparison to conventional techniques.

5.6 Conclusion

This study has demonstrated negligible tissue temperature rise during ablation of bone using a novel picosecond infrared laser (PIRL). This technology may have future significant applications in bone surgery.

5.7 Conflict of interest statement

R. Knecht is member of Advisory Boards of Merck Serono, Sanofi Aventis, Boehringer Ingelheim and Bayer Healthcare, Leverkusen. Prof RJD Miller and Dr Franjic are co-founders of AttoDyne Inc (manufacturer of the PIRL system). Prof Miller is author of a patent related to the mechanism of PIRL laser ablation.

5.8 Funding sources

This research was sponsored, in part, by a resident research grant from the American Academy of Otolaryngology - Head and Neck Surgery Foundation (AAO-HNSF) Centralized Otolaryngology Research Efforts (CORE) grant program, a Canadian Institute of Photonic Innovations (CIPI) Technology Exploitation Network (TEN) grant, a Canadian Institute of Health Research (CIHR) Banting and Best M.Sc. Award, and the McGill Faculty of Medicine Frank Litvack Clinician Scientist Fellowship.

6 Discussion

6.1 Linking statement from manuscripts

The previous two chapters detailed experiments in the form of manuscripts comparing heat generation during ablation of *ex vivo* soft and osseous using conventional microsecond Er:YAG laser ablation systems currently in clinical use with the novel PIRL system. Both studies confirmed negligible heat generation during PIRL ablation, in contrast to potentially injurious temperature levels generated during microsecond Er:YAG laser ablation. Although both systems ablate tissue primarily through photothermal vaporization, material removal by means of PIRL ablation is much more efficient since it occurs under conditions of thermal and stress confinement, which strongly enhance secondary thermoelastic photomechanical ablation mechanisms.

6.2 Future directions

Preliminary live animal studies in a murine model have already provided evidence for improved soft-tissue healing following incisions made by PIRL ablation in comparison to Er:YAG laser and traditional surgical scalpel [11]. This result must be confirmed in other live animal models that better replicate the healing properties of human skin (for example, a live porcine model). Secondly, as the healing and mechanical properties of bone are fundamentally different from those of soft-tissue, live animal studies are needed to characterize the effects efficiency of PIRL ablation of bone. Bone is a much harder and brittle material than skin; the photomechanical effects, specifically the potential injurious effect of propagation of short pulse laser generated acoustic transients must be carefully studied before any potential introduction into clinical use. Thirdly, for many clinical applications utilizing laser ablation, some degree of thermal heating is

desirable for purposes of coagulation. With current lasers in clinical use, it is not possible to independently control laser energy deposited for purposes of tissue ablation from the energy required for coagulation. The PIRL provides a means of such control when combined with a second coagulating laser beam, whose fluence can be adjusted independently to provide coagulation without excessive thermal injury. Pulsed visible lasers, such as a KTP or dye laser, emit wavelengths which are strongly absorbed by hemoglobin, leading to a subsequent intravascular photocoagulation cascade [112]. Fortunately, the addition of such a second beam to the path of the PIRL beam would be relatively straightforward to engineer.

One of the more exciting implications of genuine cold-ablation of tissue is that non-thermalized and chemically unmodified cells, cellular fragments, and proteins are ejected from the tissue surface during the ablation process. These elements may be collected, analyzed, and subsequently identified using mass spectrometry or spectroscopy techniques. Cellular or protein signals may be recognized in near real-time, proving rapid analysis of the type of tissue being ablated. Using such protein signals, software could be designed to trigger beam shutoff when critical structures such as nerves or vessels are encountered during ablation. Similarly, using tumour protein signals obtained from analysis of tumour data bank samples, the possibility exists for the use of PIRL ablation in a similar manner to how frozen sections are currently utilized to provide the surgeon with intra-operative tumour margin analysis. In this instance, a PIRL coupled to a miniaturized mass spectrometer would be used to ablate a very superficial layer of cells from a region in question in the operative field after gross tumour removal in order to identify any possible remaining microscopic disease.

7 Conclusion

This study has demonstrated that tissue temperature rise during pulsed laser ablation of soft tissue and bone is negligible for PIRL ablation while significant for microsecond Er:YAG laser ablation.

The negligible heat generation as measured during PIRL ablation confirms the potential of this novel technology in minimizing undesirable thermal injury associated with lasers currently in clinical use. This study provides evidence for genuine cold ablation of soft tissue using an ultrafast picosecond pulse infrared laser system, at fluence and irradiance levels far below the threshold for ionization or free-radical production.

7.1 Claim of originality

This is the first study to measure heat generation during ablation using the novel picosecond infrared laser system. It has confirmed by use of thermal imagery that PIRL ablation of *ex vivo* soft tissue and bone causes negligible tissue heating, far below levels that may result in cellular injury.

8 List of Abbreviations

AMaST	Ablation zone maximum surface temperature
BMeST	Baseline mean surface temperature
CO_2	Carbon dioxide
E_p	Pulse energy
ECM	Extracellular matrix
Er:Yag	Erbium-doped: yttrium aluminium garnet
Ho:YAG	Holmium: yttrium aluminium garnet
I	Laser irradiance/radiant flux density
IHDVE	Impulsive heat deposition through vibrational excitations
KTP	Potassium titanyl phosphate
L	Optical penetration depth/optical absorption length
Nd:YAG	Neodynium: yttrium aluminium garnet
P	Laser power/radiant power
PIRL	Picosecond infrared laser
TGF β	Tumour growth factor β
UTS	Ultimate tensile strength
Z_{therm}	Thermal penetration depth
τ_{ac}	Acoustic confinement/relaxation time
τ_{th}	Thermal confinement/relaxation time
τ_p	Pulse width/pulse length
τ_{pp}	Pulse-to-pulse width

$\bar{\nu}$	Spectroscopic wavenumber
WMeT	Water and airflow mean temperature
ϕ	Laser fluence/radiant exposure
λ	Wavelength

9 Bibliography

1. Eriksson, A.R., T. Albrektsson, and B. Albrektsson, *Heat caused by drilling cortical bone. Temperature measured in vivo in patients and animals.* Acta Orthop Scand, 1984. **55**(6): p. 629-31.
2. Toksvig-Larsen, S., L. Ryd, and A. Lindstrand, *On the problem of heat generation in bone cutting. Studies on the effects on liquid cooling.* J Bone Joint Surg Br, 1991. **73**(1): p. 13-5.
3. Salama, A.R., et al., *Free-flap failures and complications in an American oral and maxillofacial surgery unit.* International Journal of Oral and Maxillofacial Surgery, 2009. **38**(10): p. 1048-1051.
4. Kamineni, S., H. Ankem, and S. Sanghavi, *Anatomical considerations for percutaneous proximal humeral fracture fixation.* Injury, 2004. **35**(11): p. 1133-6.
5. Vogel, A. and V. Venugopalan, *Mechanisms of pulsed laser ablation of biological tissues.* Chem Rev, 2003. **103**(2): p. 577-644.
6. Abu-Serriah, M., et al., *Removal of partially erupted third molars using an Erbium (Er):YAG laser: a randomised controlled clinical trial.* Br J Oral Maxillofac Surg, 2004. **42**(3): p. 203-8.
7. Campbell, E.M. and Society of Photo-optical Instrumentation Engineers., *Femtosecond and nanosecond high-intensity lasers and applications : 17-18 January 1990, Los Angeles, California*. Proceedings / SPIE--the International Society for Optical Engineering. 1990, Bellingham, Wash., USA: SPIE. vii, 224 p.

8. Franjic, K., et al., *Laser selective cutting of biological tissues by impulsive heat deposition through ultrafast vibrational excitations.* Opt Express, 2009. **17**(25): p. 22937-59.

9. Mahvash, M., et al., *Modeling the forces of cutting with scissors.* IEEE transactions on bio-medical engineering, 2008. **55**(3): p. 848-56.

10. Izmailov, G.A., et al., *[Evaluation of the healing of skin wounds inflicted by steel scalpels with various degrees of sharpness]*. Khirurgiia, 1989(6): p. 75-8.

11. Amini-Nik, S., et al., *Ultrafast mid-IR laser scalpel: protein signals of the fundamental limits to minimally invasive surgery.* PLoS ONE [Electronic Resource], 2010. **5**(9).

12. Loh, S.A., et al., *Comparative healing of surgical incisions created by the PEAK PlasmaBlade, conventional electrosurgery, and a scalpel.* Plastic and Reconstructive Surgery, 2009. **124**(6): p. 1849-59.

13. Arashiro, D.S., et al., *Histologic evaluation of porcine skin incisions produced by CO2 laser, electrosurgery, and scalpel.* The International journal of periodontics & restorative dentistry, 1996. **16**(5): p. 479-91.

14. Hambley, R., et al., *Wound healing of skin incisions produced by ultrasonically vibrating knife, scalpel, electrosurgery, and carbon dioxide laser.* The Journal of dermatologic surgery and oncology, 1988. **14**(11): p. 1213-7.

15. Link, W.J., F.P. Incropera, and J.L. Glover, *A plasma scalpel: comparison of tissue damage and wound healing with electrosurgical and steel scalpels.* Archives of surgery, 1976. **111**(4): p. 392-7.

16. Pearlman, N.W., et al., *A prospective study of incisional time, blood loss, pain, and healing with carbon dioxide laser, scalpel, and electrosurgery.* Archives of surgery, 1991. **126**(8): p. 1018-20.

17. Vore, S.J., et al., *Comparative healing of surgical incisions created by a standard "bovie," the Utah Medical Epitome Electrode, and a Bard-Parker cold scalpel blade in a porcine model: a pilot study.* Annals of Plastic Surgery, 2002. **49**(6): p. 635-45.

18. Tetsch, P., *Development of raised temperature after osteotomies.* J Maxillofac Surg, 1974. **2**(2-3): p. 141-5.

19. Eriksson, A., et al., *Thermal injury to bone. A vital-microscopic description of heat effects.* International Journal of Oral Surgery, 1982. **11**(2): p. 115-21.

20. Eriksson, A.R. and T. Albrektsson, *Temperature threshold levels for heat-induced bone tissue injury: a vital-microscopic study in the rabbit.* J Prosthet Dent, 1983. **50**(1): p. 101-7.

21. Eriksson, R.A. and T. Albrektsson, *The effect of heat on bone regeneration: an experimental study in the rabbit using the bone growth chamber.* J Oral Maxillofac Surg, 1984. **42**(11): p. 705-11.

22. Battista, R.A. and P.D. Littlefield, *Revision BAHA Surgery.* Otolaryngol Clin North Am, 2006. **39**(4): p. 801-13, viii.

23. Sliney, D.H. and M.L. Wolbarsht, *Future applications of lasers in surgery and medicine: a review.* J R Soc Med, 1989. **82**(5): p. 293-6.

24. Murray, A.K. and M.R. Dickinson, *Tissue ablation-rate measurements with a long-pulsed, fibre-deliverable 308 nm excimer laser.* Lasers Med Sci, 2004. **19**(3): p. 127-38.

25. McKee, M.D., *Effects of CO2 laser irradiation in vivo on rat alveolar bone and incisor enamel, dentin, and pulp.* J Dent Res, 1993. **72**(10): p. 1406-17.

26. Einstein, A., *Quantum theory of radiation.* Physikalische Zeitschrift, 1917. **18**: p. 121-128.

27. Maiman, T.H., *Stimulated Optical Radiation in Ruby.* Nature, 1960. **187**(4736): p. 493-494.

28. Niemz, M.H., *Laser-tissue interactions : fundamentals and applications*. 3rd, enlarged ed. Biological and medical physics, biomedical engineering,. 2007, Berlin, Heidelberg: Springer-Verlag. xvi, 305 p.

29. Boulnois, J.-L., *Photophysical processes in recent medical laser developments: A review.* Lasers in Medical Science, 1986. **1**(1): p. 47-66.

30. Franjic, K. and R.J.D. Miller, *Vibrationally excited ultrafast thermodynamic phase transitions at the water/air interface.* Physical Chemistry Chemical Physics, 2010. **12**(20): p. 5225-5239.

31. Apitz, I. and A. Vogel, *Material ejection in nanosecond Er:YAG laser ablation of water, liver, and skin.* Applied Physics A, 2005. **81**(2): p. 329-338.

32. Puliafito, C.A. and R.F. Steinert, *Short-Pulsed Nd-Yag Laser Microsurgery of the Eye - Biophysical Considerations.* Ieee Journal of Quantum Electronics, 1984. **20**(12): p. 1442-1448.

33. Vogel, A., et al., *Energy balance of optical breakdown in water at nanosecond to femtosecond time scales.* Applied Physics B-Lasers and Optics, 1999. **68**(2): p. 271-280.

34. Pauling, L., *Die Natur der chemischen Bindung*. 1962, Weinheim: Verlag Chemie.

35. Segelstein, D.J. and M.R. Querry, *The complex refractive index of water*. 1981, Department of Physics. University of Missouri-Kansas City. p. ix, 167 leaves.

36. Schenkman, K.A., *Visible and Near Infrared Absorption Spectra of Human and Animal Haemoglobin.* Critical Care Medicine, 2002. **30**(1): p. 267.

37. Prahl, S.A., *Light transport in tissue,* in *Department of Physics*. 1988, The University of Texas at Austin: Austin, Texas.

38. van Veen, R.L.P., et al., *Determination of visible near-IR absorption coefficients of mammalian fat using time- and spatially resolved diffuse reflectance and transmission spectroscopy.* Journal of Biomedical Optics, 2005. **10**(5).

39. Pettit, G.H. and M.N. Ediger, *Corneal-tissue absorption coefficients for 193- and 213-nm ultraviolet radiation.* Applied Optics, 1996. **35**(19): p. 3386-3391.

40. Jacques, S.L., *Role of tissue optics and pulse duration on tissue effects during high-power laser irradiation.* Appl Opt, 1993. **32**(13): p. 2447-54.

41. Hayes, J.R. and M.L. Wolbarsht, *Thermal model for retinal damage induced by pulsed lasers.* Aerosp Med, 1968. **39**(5): p. 474-80.

42. Paltauf, G. and P.E. Dyer, *Photomechanical processes and effects in ablation.* Chemical Reviews, 2003. **103**(2): p. 487-518.

43. Dingus, R.S. and R.J. Scammon. *Grüneisen-stress-induced ablation of biological tissue*. 1991. Los Angeles, CA, USA: SPIE.

44. Walsh, J.T., Jr. and T.F. Deutsch, *Er:YAG laser ablation of tissue: measurement of ablation rates.* Lasers Surg Med, 1989. **9**(4): p. 327-37.

45. Walsh, J.T., Jr., et al., *Pulsed CO2 laser tissue ablation: effect of tissue type and pulse duration on thermal damage.* Lasers in Surgery and Medicine, 1988. **8**(2): p. 108-18.

46. Verdaasdonk, R.M., C. Borst, and M.J. van Gemert, *Explosive onset of continuous wave laser tissue ablation.* Phys Med Biol, 1990. **35**(8): p. 1129-44.

47. Srinivasan, R. and W.J. Leigh, *Ablative Photo-Decomposition - Action of Far Ultraviolet (193-Nm) Laser-Radiation on Poly(Ethylene-Terephthalate) Films.* Journal of the American Chemical Society, 1982. **104**(24): p. 6784-6785.

48. Kawamura, Y., K. Toyoda, and S. Namba, *Effective Deep Ultraviolet Photoetching of Poly(Methyl Methacrylate by an Excimer Laser.* Applied Physics Letters, 1982. **40**(5): p. 374-375.

49. Garrison, B.J. and R. Srinivasan, *Ablative Photodecomposition of Polymers.* Journal of Vacuum Science & Technology a-Vacuum Surfaces and Films, 1985. **3**(3): p. 746-748.

50. Srinivasan, R., *Ablation of Polymers and Biological Tissue by Ultraviolet-Lasers.* Science, 1986. **234**(4776): p. 559-565.

51. Schmidt, H., et al., *Ultraviolet laser ablation of polymers: spot size, pulse duration, and plume attenuation effects explained.* Journal of Applied Physics, 1998. **83**(10): p. 5458-5468.

52. Noack, J. and A. Vogel, *Laser-induced plasma formation in water at nanosecond to femtosecond time scales: Calculation of thresholds, absorption coefficients, and energy density.* Ieee Journal of Quantum Electronics, 1999. **35**(8): p. 1156-1167.

53. Mao, S.S., et al., *Dynamics of femtosecond laser interactions with dielectrics.* Applied Physics A: Materials Science & Processing, 2004. **79**(7): p. 1695-1709.

54. Niemz, M.H., E.G. Klancnik, and J.F. Bille, *Plasma-mediated ablation of corneal tissue at 1053 nm using a Nd:YLF oscillator/regenerative amplifier laser.* Lasers Surg Med, 1991. **11**(5): p. 426-31.

55. Stern, D., et al., *Corneal ablation by nanosecond, picosecond, and femtosecond lasers at 532 and 625 nm.* Arch Ophthalmol, 1989. **107**(4): p. 587-92.

56. Margetic, V., et al., *A comparison of nanosecond and femtosecond laser-induced plasma spectroscopy of brass samples.* Spectrochimica Acta Part B: Atomic Spectroscopy, 2000. **55**(11): p. 1771-1785.

57. Chichkov, B.N., et al., *Femtosecond, picosecond and nanosecond laser ablation of solids.* Applied Physics A: Materials Science & Processing, 1996. **63**(2): p. 109-115.

58. Sallé, B., et al., *Femtosecond and picosecond laser microablation: ablation efficiency and laser microplasma expansion.* Applied Physics A: Materials Science & Processing, 1999. **69**(7): p. S381-S383.

59. Chowdhury, I.H., et al., *Ultra-fast laser absorption and ablation dynamics in wide-band-gap dielectrics.* Applied Physics A: Materials Science & Processing, 2005. **81**(8): p. 1627-1632.

60. Girard, B., et al., *Effects of femtosecond laser irradiation on osseous tissues.* Lasers in Surgery and Medicine, 2007. **39**(3): p. 273-285.

61. Girard, B., et al., *Microtomographic analysis of healing of femtosecond laser bone calvarial wounds compared to mechanical instruments in mice with and without application of BMP-7.* Lasers Surg Med, 2007. **39**(5): p. 458-67.

62. Tirlapur, U.K., et al., *Femtosecond near-infrared laser pulses elicit generation of reactive oxygen species in mammalian cells leading to apoptosis-like death.* Exp Cell Res, 2001. **263**(1): p. 88-97.

63. Srinivasan, R., B. Braren, and K.G. Casey, *Ultraviolet-Laser Ablation and Decomposition of Organic Materials.* Pure and Applied Chemistry, 1990. **62**(8): p. 1581-1584.

64. Srinivasan, R., et al., *Mechanism of the Ultraviolet-Laser Ablation of Poly(Methyl Methacrylate at 193 and 248 Nm - Laser-Induced Fluorescence Analysis, Chemical-Analysis, and Doping Studies.* Journal of the Optical Society of America B-Optical Physics, 1986. **3**(5): p. 785-791.

65. Vogel, A., et al., *Intraocular Nd-Yag Laser-Surgery - Light Tissue Interaction, Damage Range, and Reduction of Collateral Effects.* Ieee Journal of Quantum Electronics, 1990. **26**(12): p. 2240-2260.

66. Doukas, A.G. and T.J. Flotte, *Physical characteristics and biological effects of laser-induced stress waves.* Ultrasound Med Biol, 1996. **22**(2): p. 151-64.

67. Frenz, M., et al., *Starting mechanisms and dynamics of bubble formation induced by a Ho:Yttrium aluminum garnet laser in water.* Journal of Applied Physics, 1998. **84**(11): p. 5905-5912.

68. Vogel, A., et al., *Cavitation Bubble Dynamics and Acoustic Transient Generation in Ocular Surgery with Pulsed Neodymium - Yag Lasers.* Ophthalmology, 1986. **93**(10): p. 1259-1269.

69. Paltauf, G., H. Schmidt-Kloiber, and M. Frenz, *Photoacoustic waves excited in liquids by fiber-transmitted laser pulses.* Journal of the Acoustical Society of America, 1998. **104**(2): p. 890-897.

70. Li, Z.Z., J.E. Code, and W.P. Van De Merwe, *Er:YAG laser ablation of enamel and dentin of human teeth: determination of ablation rates at various fluences and pulse repetition rates.* Lasers Surg Med, 1992. **12**(6): p. 625-30.

71. Martins, G.L., et al., *Bone healing after bur and Er:YAG laser ostectomies.* Journal of Oral & Maxillofacial Surgery, 2011. **69**(4): p. 1214-20.

72. Lundy, L., *The Effect of CO(2) and KTP laser on the cat saccule and utricle.* Laryngoscope, 2009. **119**(8): p. 1594-605.

73. Marchese, M.R., et al., *"One-shot" CO2 versus Er:YAG laser stapedotomy: is the outcome the same?* European Archives of Oto-Rhino-Laryngology, 2011. **268**(3): p. 351-6.

74. Nagel, D., *The Er:YAG laser in ear surgery: first clinical results.* Lasers in Surgery and Medicine, 1997. **21**(1): p. 79-87.

75. Qiao, Y., et al., *[Analysis of the short-term and long-term effect of Er-yttrium aluminum garnet laser in stapes surgery]*. Zhonghua Er Bi Yan Hou Tou Jing Wai Ke Za Zhi = Chinese Journal of Otorhinolaryngology Head & Neck Surgery, 2009. **44**(5): p. 359-63.

76. Timoshenko, A.P., et al., *A comparison of the hearing results of KTP and Erbium YAG laser stapedotomy.* Acta Oto-Laryngologica, 2009. **129**(2): p. 217-9.

77. Carome, E.F., N.A. Clark, and C.E. Moeller, *Generation of Acoustic Signals in Liquids by Ruby Laser-Induced Thermal Stress Transients (Effect of Acoustic Boundary Condition on Impulse Shape E/T D.* Applied Physics Letters, 1964. **4**(6): p. 95-&.

78. Itzkan, I., et al., *The Thermoelastic Basis of Short Pulsed-Laser Ablation of Biological Tissue.* Proceedings of the National Academy of Sciences of the United States of America, 1995. **92**(6): p. 1960-1964.

79. Itzkan, I., D. Albagli, and M.S. Feld, *Inertially Confined Ablation of Biological Tissue.* Leos '93 Conference Proceedings, 1993: p. 230-231.

80. Albagli, D., et al., *Photomechanical Basis of Laser-Ablation of Biological Tissue.* Optics Letters, 1994. **19**(21): p. 1684-1686.

81. Paltauf, G. and H. Schmidt-Kloiber, *Model study to investigate the contribution of spallation to pulsed laser ablation of tissue.* Lasers Surg Med, 1995. **16**(3): p. 277-87.

82. Venugopalan, V., N.S. Nishioka, and B.B. Mikic, *Thermodynamic response of soft biological tissues to pulsed infrared-laser irradiation.* Biophysical Journal, 1996. **70**(6): p. 2981-2993.

83. Vodopyanov, K.L., et al., *Laser-Induced Generation of Subnanosecond Sound Pulses in Liquids.* Zhurnal Eksperimentalnoi I Teoreticheskoi Fiziki, 1986. **91**(1): p. 114-121.

84. Zweig, A.D., *A Thermomechanical Model for Laser Ablation.* Journal of Applied Physics, 1991. **70**(3): p. 1684-1691.

85. Pan, T.L., et al., *Systematic evaluations of skin damage irradiated by an erbium:YAG laser: histopathologic analysis, proteomic profiles, and cellular response.* Journal of dermatological science, 2010. **58**(1): p. 8-18.

86. Walsh, J.T., Jr., T.J. Flotte, and T.F. Deutsch, *Er:YAG laser ablation of tissue: effect of pulse duration and tissue type on thermal damage.* Lasers in Surgery and Medicine, 1989. **9**(4): p. 314-26.

87. Alster, T.S. and J.R. Lupton, *Erbium:YAG cutaneous laser resurfacing.* Dermatologic clinics, 2001. **19**(3): p. 453-66.

88. Weinstein, C., *Erbium laser resurfacing: current concepts.* Plastic and Reconstructive Surgery, 1999. **103**(2): p. 602-16; discussion 617-8.

89. Cowan, M.L., et al., *Ultrafast memory loss and energy redistribution in the hydrogen bond network of liquid H2O.* Nature, 2005. **434**(7030): p. 199-202.

90. Planck, M. and M. Masius, *The theory of heat radiation*. 1914: P. Blakiston's son & co. xiv, p., 1 l., 225 p. diagrs.

91. Gao, Y.S., J.T. Su, and Y.B. Yan, *Sequential events in the irreversible thermal denaturation of human brain-type creatine kinase by spectroscopic methods.* International journal of molecular sciences, 2010. **11**(7): p. 2584-96.

92. Dekhtyar, Y., et al., *Electron and mechanical properties of bone during heating, evaluated by exoelectron emission and ultrasound.* Biomaterials, 1995. **16**(11): p. 861-3.

93. Arnoczky, S.P. and A. Aksan, *Thermal modification of connective tissues: basic science considerations and clinical implications.* The Journal of the American Academy of Orthopaedic Surgeons, 2000. **8**(5): p. 305-13.

94. Speka, M., et al., *The infrared thermography control of the laser welding of amorphous polymers.* Ndt & E International, 2008. **41**(3): p. 178-183.

95. *Non-destructive inspection using laser-ultrasound and infrared thermography.* Materials Evaluation, 2012. **70**(2): p. 143-144.

96. Brunsmann, U., et al., *Evaluation of thermal load during laser corneal refractive surgery using infrared thermography.* Infrared Physics & Technology, 2010. **53**(5): p. 342-347.

97. Mattei, S., et al., *Using infrared thermography in order to compare laser and hybrid (laser plus MIG) welding processes.* Optics and Laser Technology, 2009. **41**(6): p. 665-670.

98. Didierjean, J., et al., *Thermal conductivity measurements of laser crystals by infrared thermography. Application to Nd: doped crystals.* Optics Express, 2008. **16**(12): p. 8995-9010.

99. Kadolkar, P.B., et al., *Thermal measurements during laser surface engineering using infrared thermography.* Surface Engineering: Coating and Heat Treatments, Proceedings, 2003: p. 229-236.

100. Thomas, R.A., et al., *Optimised laser application in dermatology using infrared thermography.* Thermosense Xxiv, 2002. **4710**: p. 424-434.

101. Choi, B., et al., *Imaging of the irradiation of skin with a clinical CO2 laser system: implications for laser skin resurfacing.* Lasers in Surgery and Medicine, 1998. **23**(4): p. 185-93.

102. Riggs, K., M. Keller, and T.R. Humphreys, *Ablative laser resurfacing: high-energy pulsed carbon dioxide and erbium:yttrium-aluminum-garnet.* Clinics in Dermatology, 2007. **25**(5): p. 462-73.

103. Stuzin, J.M., T.J. Baker, and T.M. Baker, *CO2 and erbium:YAG laser resurfacing: current status and personal perspective.* Plastic and Reconstructive Surgery, 1999. **103**(2): p. 588-91.

104. Selting, W.J., *Fundamental Erbium Laser Concepts: Part I.* J Laser Dent, 2009. **17**(2): p. 87-93.

105. Selting, W.J., *Fundatmental Erbium Laser Concepts: Part II.* J Laser Dent, 2010. **18**(3): p. 116-122.

106. el Montaser, M.A., et al., *Pattern of healing of calvarial bone in the rat following application of the erbium-YAG laser.* Lasers Surg Med, 1997. **21**(3): p. 255-61.

107. Nelson, J.S., et al., *Mid-infrared erbium:YAG laser ablation of bone: the effect of laser osteotomy on bone healing.* Lasers Surg Med, 1989. **9**(4): p. 362-74.

108. Apel, C., et al., *The ablation threshold of Er:YAG and Er:YSGG laser radiation in dental enamel.* Lasers Med Sci, 2002. **17**(4): p. 246-52.

109. Böttcher, A., et al., *A Novel Tool in Laryngeal Surgery - Preliminary Results of the Picosecond Infrared Laser (PIRL).* Laryngoscope (in press), 2013.

110. Jowett, N., et al., *Heat generation during ablation of porcine skin with Er:YAG laser versus a novel picosecond infrared laser (PIRL).* JAMA Otolaryngology - Head & Neck Surgery. **(in press)**.

111. Colucci, V., et al., *Water flow on erbium:yttrium-aluminum-garnet laser irradiation: effects on dental tissues.* Lasers Med Sci, 2009. **24**(5): p. 811-8.

112. Black, J.F. and J.K. Barton, *Chemical and structural changes in blood undergoing laser photocoagulation.* Photochem Photobiol, 2004. **80**: p. 89-97.